TISSUE ENGINEERING

Tissue engineered autologous cartilage-bone grafts for temporomandibular joint regeneration

David Chen[1]*, Josephine Y. Wu[1]*, Kelsey M. Kennedy[1], Keith Yeager[1], Jonathan C. Bernhard[1], Johnathan J. Ng[1], Brandon K. Zimmerman[2], Samuel Robinson[1], Krista M. Durney[1], Courtney Shaeffer[2], Olaia F. Vila[1], Catherine Takawira[3], Jeffrey M. Gimble[4], X. Edward Guo[1], Gerard A. Ateshian[1,2], Mandi J. Lopez[3], Sidney B. Eisig[5], Gordana Vunjak-Novakovic[1,5,6†]

Joint disorders can be detrimental to quality of life. There is an unmet need for precise functional reconstruction of native-like cartilage and bone tissues in the craniofacial space and particularly for the temporomandibular joint (TMJ). Current surgical methods suffer from lack of precision and comorbidities and frequently involve multiple operations. Studies have sought to improve craniofacial bone grafts without addressing the cartilage, which is essential to TMJ function. For the human-sized TMJ in the Yucatan minipig model, we engineered autologous, biologically, and anatomically matched cartilage-bone grafts for repairing the ramus-condyle unit (RCU), a geometrically intricate structure subjected to complex loading forces. Using image-guided micromilling, anatomically precise scaffolds were created from decellularized bone matrix and infused with autologous adipose-derived chondrogenic and osteogenic progenitor cells. The resulting constructs were cultured in a dual perfusion bioreactor for 5 weeks before implantation. Six months after implantation, the bioengineered RCUs maintained their predefined anatomical structure and regenerated full-thickness, stratified, and mechanically robust cartilage over the underlying bone, to a greater extent than either autologous bone-only engineered grafts or acellular scaffolds. Tracking of implanted cells and parallel bioreactor studies enabled additional insights into the progression of cartilage and bone regeneration. This study demonstrates the feasibility of TMJ regeneration using anatomically precise, autologous, living cartilage-bone grafts for functional, personalized total joint replacement. Inclusion of the adjacent tissues such as soft connective tissues and the TMJ disc could further extend the functional integration of engineered RCUs with the host.

INTRODUCTION

The temporomandibular joint (TMJ) is a complex and highly loaded joint implicated in many craniofacial diseases and disorders. It is estimated that 10 million people in the United States alone suffer from TMJ dysfunction (*1*). In severe cases, surgical reconstruction is the only option to treat pain and restore function. The need for reconstruction may result from congenital defects such as hemifacial microsomia, damage to the joint due to traumatic injuries or neoplasms, or resorption of the joint due to arthritis, juvenile inflammatory arthritis, or idiopathic condylar resorption (*2*). All current treatments have limitations. Steroid injections only provide temporary relief, with some patients experiencing recurring pain within 2 months (*3*). Surgical interventions, such as condylectomy, that are most commonly used for condylar hyperplasia produce varying results and do not fully restore TMJ function (*4*–*6*). Patients who receive condylectomy tend to experience more TMJ problems and postoperative pain compared to untreated patients (*7*). Autologous transplants such as costochondral grafts and fibular flaps, mostly used for large mandibular defects, are limited by the geometry and volume of donor tissue and donor site morbidity (*8*, *9*). Last, synthetic options are not without problems. The Teflon-Proplast total joint replacement induced foreign-body giant cell reactions in most patients, with erosions of the glenoid fossa sometimes extending into the middle cranial fossa, and this prosthesis was pulled from the market more than 30 years ago (*10*, *11*). The more recent Zimmer Biomet stock prosthesis and TMJ Concepts patient-matched device have shown early success, but future studies with larger cohorts are needed to assess long-term outcomes, particularly the effects of altered joint loading with alloplastic replacements (*12*, *13*). More recently, metal hypersensitivity and nickel allergy have caused concern among surgeons using these systems, with up to 17% of individuals having metal allergies (*14*, *15*). Metal hypersensitivity to an implanted joint prosthesis can manifest as localized dermatitis, swelling, pain, joint effusions, and prosthesis failure. Together, these considerations make the development of an autologous, bioengineered mandibular condyle joint replacement all the more compelling (*16*).

Engineered tissue constructs offer bioinspired and patient-tailored approaches to the reconstruction of the structural and biological components of the graft. Initial efforts have focused on the tissue-engineered bone for the mandible. One recent study proposed an "in vivo bioreactor" strategy for repair of a large mandibular defect in a sheep model, allowing the engineered bone to develop against the rib periosteum before reconstruction of the defect (*17*). Another study in an ovine model developed precise customized synthetic grafts loaded with hydroxyapatite for replacement of the orbital floor, resulting in neovascularization and bone morphogenesis (*18*). Our group previously reported a translational study in Yucatan minipigs, in which we engineered anatomically correct autologous bone grafts for reconstructing the ramus-condyle unit (RCU). The engineered bone showed regenerative advantage over acellular scaffolds, suggesting that the autologous stromal/stem cells incorporated in the grafts contributed to successful integration and tissue regeneration.

[1]Department of Biomedical Engineering, Columbia University, New York, NY 10032, USA. [2]Department of Mechanical Engineering, Columbia University, New York, NY 10032, USA. [3]School of Veterinary Medicine, Louisiana State University, Baton Rouge, LA 70803, USA. [4]LaCell LLC and Obatala Sciences, New Orleans, LA 70148, USA. [5]College of Dental Medicine, Columbia University, New York, NY 10032, USA. [6]Department of Medicine, Columbia University, New York, NY 10032, USA.
*These authors contributed equally to this work.
†Corresponding author. Email: gv2131@columbia.edu

Consistently, the rates of bone resorption and replacement appeared more balanced in cellular than acellular engineered grafts (*19*, *20*).

Few studies have focused on reconstruction strategies that incorporate a cartilage layer over the underlying bone. The condylar cartilage of the TMJ is essential to its mechanical function, providing resistance to compressive loading and frictionless articulation. In therapeutic approaches to TMJ repair, cartilage regeneration is often the central goal, because the cartilage is the tissue being degraded under conditions of arthritis or idiopathic condylar resorption. However, many studies have demonstrated repair of defects more distal from the condylar head, because of the lack of techniques to engineer both the cartilage and bone together in one construct to enable total joint repair. In our previous work, implanting engineered bone-only RCU grafts in pigs resulted in the formation of a thin layer of cartilaginous tissue on the condylar head, but this tissue lacked the zonal organization, biochemical composition, and low friction coefficient of the native TMJ condylar cartilage (*19*). Several studies have demonstrated repair of small, localized cartilage defects but do not offer scalability for in vivo regeneration of the whole condylar head (*21*–*23*). The TMJ cartilage also has a distinct structure compared to the hyaline cartilage, with a superficial fibrous layer above proliferative and hypertrophic zones.

Our goal was to overcome the common limitation of previous studies—the lack of mature, stratified cartilage layers that can restore TMJ function in large defects and total joint replacement procedures. To this end, we report the engineering and implantation of autologous, anatomically correct RCUs with the stratified cartilage interfacing the underlying bioengineered living bone to achieve TMJ regeneration. The performance of cartilage-bone RCUs for TMJ replacement was demonstrated in the Yucatan minipig, an animal model with human-sized TMJ and adequate jaw anatomy, loading, and remodeling (*24*–*26*). We compared the performance of anatomically precise cartilage-bone grafts to that of bone-only grafts and acellular scaffolds, hypothesizing that the inclusion of a cartilage precursor leads to improved graft quality. We advanced the design and capabilities of our previously established bioreactors for cultivation of the anatomically shaped bone (*19*, *27*) into a dual perfusion bioreactor for cultivation of an anatomically correct RCU composed of cartilage and bone regions formed from the same autologous population of adipose-derived stromal/stem cells (ASCs). This complex tissue graft was evaluated against contralateral native tissues, bone-only grafts without a cartilage region, and acellular scaffolds over 6 months of orthotopic implantation in a clinically sized animal model. We also investigated the roles of implanted cells in the progression of cartilage and bone regeneration via cell tracking in vivo and parallel bioreactor studies.

RESULTS

Dual perfusion bioreactors enable development of cartilage-bone RCUs

Our objective was to engineer autologous cartilage-bone RCUs with patient-specific geometry at a clinically translatable scale. To this end, we used anatomically matched decellularized bone matrix scaffolds, autologous ASCs, and dual perfusion bioreactors with separate compartments and culture media for bone and cartilage cultivation (Fig. 1A). For comparison, we also used a similar process to engineer bone-only RCUs in a single perfusion bioreactor, as previously described (*19*). To better understand the processes contributing to tissue development, we engineered additional small cylindrical constructs with representative curvature of the articulating surface and investigated these constructs in bioreactor studies, in parallel with the clinically sized cartilage-bone and bone-only RCUs (Fig. 1B). The cartilage-bone RCUs and their small-size counterparts were cultured in the dual-tissue perfusion bioreactors for 5 weeks (Fig. 1C).

Scaffolds were derived from the trabecular bone of bovine distal femurs, completely decellularized (*19*), and milled into anatomically precise replicas of each animal's RCU based on computed tomography (CT)–guided reconstructions, with each RCU measuring about 3 cm in width by 6 cm in length and 0.7 cm in thickness at the base and 2.5 cm in thickness at the condylar head. For the smaller constructs, scaffold dimensions (9-mm diameter and 9-mm height) and surface curvature were chosen such that they would be representative of a core taken from the center of the condylar head of the RCU.

For each animal, we isolated ASCs from a small subcutaneous adipose biopsy and expanded the cells to sufficient numbers. No bone morphogenic proteins nor any other growth factors were used for osteogenic culture. For cartilage formation, condensed mesenchymal bodies were formed from the ASCs and seeded onto the RCUs as previously described (*21*). The only growth factor used for chondrogenic culture was transforming growth factor–β (TGF-β), which is known to be critical for chondrogenic induction (*28*). ASCs from each animal were added to the corresponding scaffold, except for the scaffolds that served as acellular controls. Scaffolds for the small constructs were seeded at the same densities as their larger counterparts, using a heterogeneous population of ASCs from several animals to normalize for biological differences between experimental groups.

Dual perfusion bioreactors were fabricated to match the graft geometry of each animal (Fig. 2, A to D). The bioreactors supported the cultivation of cartilage-bone RCUs by enabling sufficient transport of nutrients, oxygen, and metabolites while also providing separate physical cues and culture media for each tissue type, because the cartilage and bone require different culture conditions. Low hydrodynamic shear has been shown to result in better cartilaginous tissue (*22*), whereas higher hydrodynamic shears induced by interstitial velocities in the bone favor osteogenic maturation (*19*, *27*). Using computational flow simulation, the number, placement, and diameter of bioreactor channels were designed to achieve perfusion velocities ranging from 400 to 1200 μm/s, depending on the graft thickness at each channel (fig. S1A and movie S1). Thorough and rapid perfusion of the scaffold without leaks was confirmed experimentally by flowing medium through the bone in the bioreactor before adding cells (fig. S1, B to D, and movie S2). A 1-μm porous polycarbonate membrane between the condylar surface and perfusion channels was placed to shield the neocartilage and reduce shear forces to negligible rates while allowing for medium exchange. To provide tissue-specific chemical cues, chondrogenic or osteogenic culture media were distributed to the appropriate regions of the RCU via separate fluid flow loops (fig. S1E). Single perfusion bioreactors for the bone-only RCUs were similarly fabricated and validated computationally and experimentally to promote osteogenic maturation (Fig. 2, E to H). Additional dual and single perfusion bioreactors were designed for the small constructs (cartilage-bone and bone-only) such that each tissue type experienced the optimal range of hydrodynamic shear, corresponding to that in the bioreactors for the larger RCUs (Fig. 2, I to K; fig. S1, F to I; and movies S3 and S4).

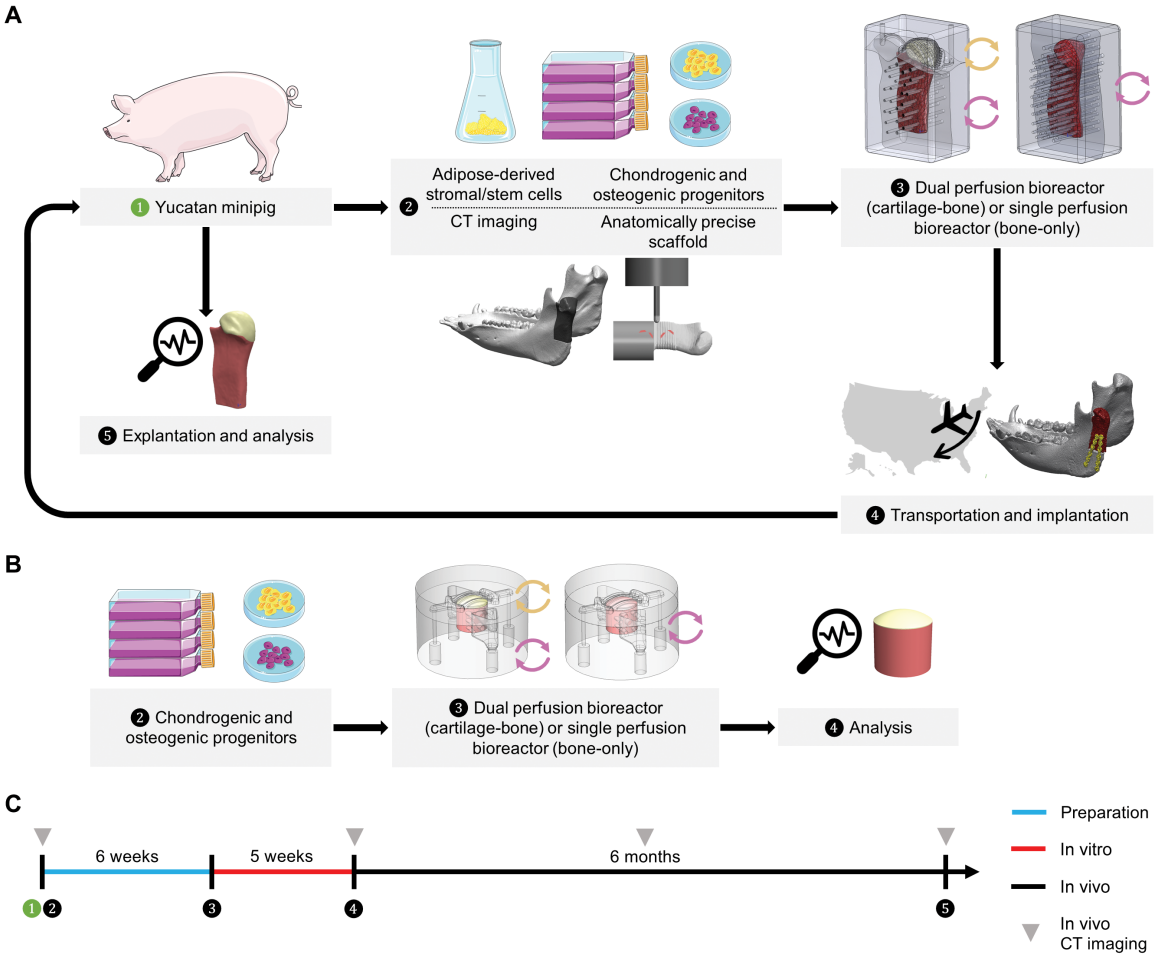

Fig. 1. Tissue engineering strategy and timeline. (**A**) Twenty Yucatan minipigs were housed in Baton Rouge, LA and allowed to reach skeletal maturity. CT imaging of the skull enabled the creation of anatomically precise scaffolds and bioreactor culture chambers. Autologous ASCs were expanded and differentiated into chondrogenic and osteogenic progenitors. Each decellularized bovine scaffold (~3 cm in width by 6 cm in length by 7 to 25 mm in thickness) was seeded with cells from the corresponding animal and cultured in a dual perfusion bioreactor to form a graft. Experimental groups were cartilage-bone (seeded with ~200 million chondrogenic progenitors and ~120 million osteogenic progenitors), bone-only (seeded with osteogenic progenitors only), and acellular (decellularized scaffold only) RCUs. RCUs were transported from New York, NY to Baton Rouge, LA and orthotopically implanted. After 6 months, the RCUs and the native contralateral tissues were excised and analyzed. (**B**) Smaller-scale cylindrical constructs (~9 mm in diameter and height) were engineered to correspond to a core taken from the center of the RCU condyle to be used for time point analyses. Cell and scaffold sources were the same as in (A). (**C**) Timeline of the steps in (A) and (B), including time points at which whole-jaw CT imaging was performed.

After 5 weeks of culture, the small cartilage-bone constructs formed neocartilage (Fig. 2L). The RCU bioreactors were shipped from the Columbia University in New York, NY, where the grafts were grown, to Louisiana State University in Baton Rouge, LA, where the animals were housed. During transport between these geographically distant sites, perfusion was discontinued for up to 10 hours. Previous computational modeling from our group of oxygen transport and consumption in RCUs of comparable dimensions indicated that the oxygen concentration after 10 hours within the RCUs was sufficient for cell survival (*19*). The large RCUs were then implanted into recipient animals. The cellularity after transportation was not notably different from the cellularity before transportation in large grafts (*19*). The RCUs remained implanted for 6 months and were subsequently analyzed by histological staining, biochemical assays, mechanical testing, and CT and micro-CT (μCT) imaging; small constructs were used for time point analyses of in vitro development. The safety of the procedure and biocompatibility of the grafts were confirmed by pig weights over the duration of study (table S1) and the complete blood count and serum chemistry panels that were consistent with physiologic variation and after operative inflammation and healing (tables S2 and S3).

Engineered cartilage in RCUs recapitulates key features of native TMJ cartilage

After 5 weeks of culture, alcian blue staining in pentachrome sections showed glycosaminoglycan (GAG) expression in the neocartilage on the condylar surface of the small cartilage-bone constructs, whereas only minimal GAG expression was found in the small bone-only constructs (Fig. 3A). After 6 months in vivo, the macroscopic quality of the cartilage in each engineered RCU was compared immediately after dissection to the same animal's native RCU on the contralateral side. Intact TMJ disc and synovial fluid were found in nearly all samples by visual inspection (fig. S2). The appearance of the cartilage and the shape of the joint were best recapitulated

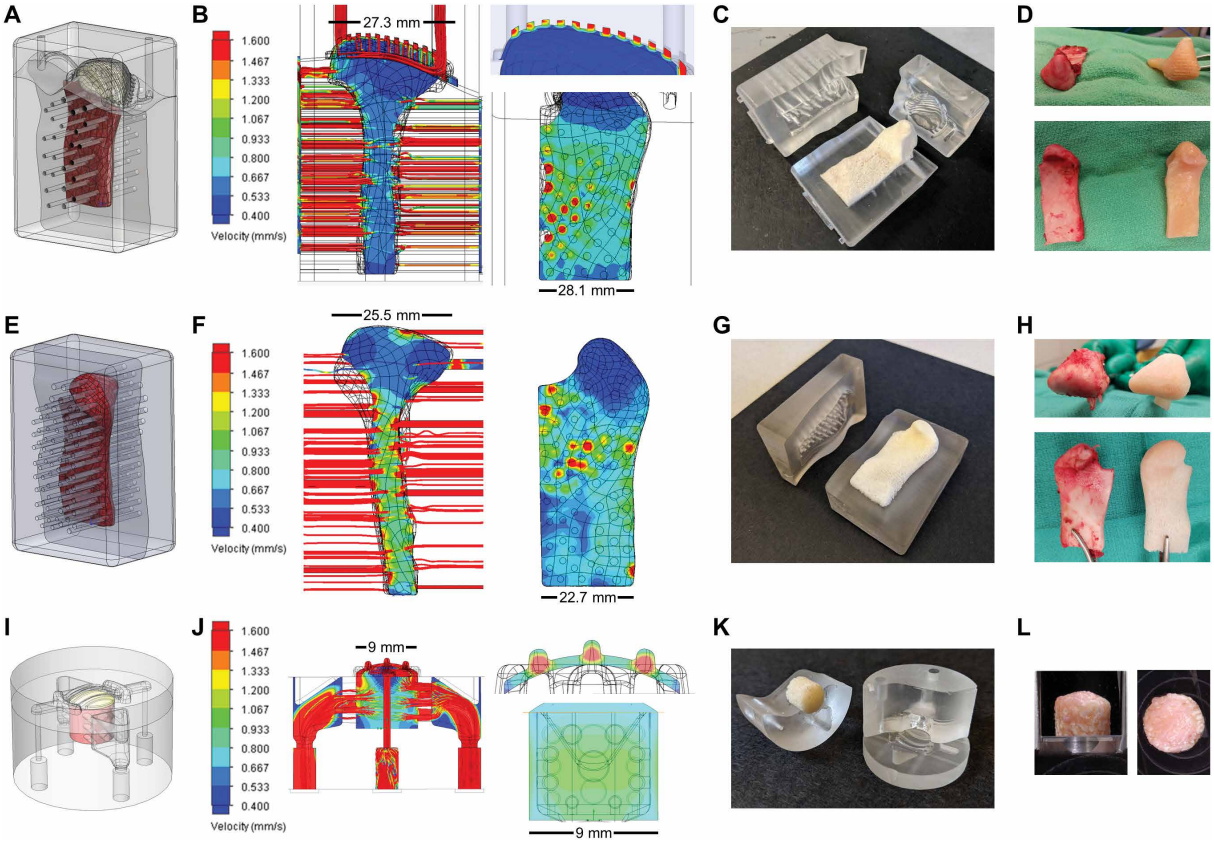

Fig. 2. Bioreactor cultivation of engineered grafts. Left to right: Schematics showing engineered grafts in bioreactor culture chambers with perfusion channels; simulated equilibrium flow rates in cartilage and bone components; preculture photographs demonstrating the precise fit of scaffolds within elastomer blocks, which form the inner bioreactor culture chamber; and postculture photographs of engineered RCUs and the corresponding excised native RCU at time of surgery or the small cylindrical constructs. (**A** to **D**) Dual perfusion bioreactor design and modeling for anatomical cartilage-bone RCUs (~3 cm in width by 6 cm in length by 7 to 25 mm in thickness). (**E** to **H**) Single perfusion bioreactor design and modeling for anatomical bone-only RCUs. (**I** to **L**) Scaled-down cartilage-bone bioreactor for small cylindrical constructs, about 9 mm in diameter.

in the cartilage-bone group and were the least native-like in the acellular control group (Fig. 3B and fig. S3).

The 6-month postimplantation engineered cartilage-bone RCUs closely recapitulated the native samples with respect to overall cartilage thickness and the presence of distinct and typical cartilage zones (Fig. 3B and fig. S3). Moving from the superficial surface to the subchondral bone, the fibrous, proliferative, hypertrophic, and calcified zones were established. Unlike the hyaline cartilage on other joints, the porcine TMJ cartilage is known to have a fibrous superficial layer dominated by collagen I (*29*). These stratified layers are important for recapitulating the functional responses of the cartilage under compressive and shear loading. In contrast, the bone-only RCUs and acellular samples were mostly dominated by a fibrous layer and lacked the requisite proliferative and hypertrophic zones. The relative layer thicknesses of the native samples were more closely matched in the cartilage-bone group (all zones, not significant) than in the bone-only and acellular groups (all zones, $P < 0.05$) (Fig. 3C). The inclusion of chondrogenic precursors during RCU cultivation in vitro ultimately resulted in better cartilage regeneration after 6 months of orthotopic implantation. The acellular controls exhibited worse morphology and cartilage could not be reliably sampled, and therefore, subsequent cartilage analyses focused on elucidating the differences among the cellularized grafts and native tissue.

In terms of biochemical composition, GAG, DNA, and hydroxyproline (OHP) values matched well with previous data for the porcine mandibular condylar cartilage (*30*). GAG content normalized to wet weight was significantly higher in native tissue (11.2 ± 2.6 μg/mg) than in cartilage-bone explants (8.8 ± 3.2 μg/mg; $P < 0.05$) or bone-only explants (7.9 ± 3.3 μg/mg; $P < 0.01$) 6 months after implantation (Fig. 3D). DNA and OHP expression showed no significant difference across experimental groups (Fig. 3, E and F). Stains for collagen II, the predominant solid component of the hyaline cartilage (*31*) and the deeper zone mandibular condylar cartilage (*32*), were comparably strong in condylar sagittal cross sections from the cartilage-bone and native groups but noticeably weaker in the bone-only group (fig. S4). Although the OHP assay found no difference in total collagen content between groups, stains for collagen I, the dominant component of the fibrous cartilage (*29*, *33*), appeared to be most prominent in the bone-only group, but relatively less present in the cartilage-bone and native groups, as determined from qualitative analysis. Additional stains for the hyaline cartilage markers aggrecan, runt-related transcription factor 2 (RUNX2), and SRY-box transcription factor 9 (SOX9) were closer to native expression in the cartilage-bone group than the bone-only group (fig. S4).

Material properties of the condylar tissues excised after 6 months in vivo were determined via compressive creep testing. Computational cartilage-bone models with sample-specific geometry were

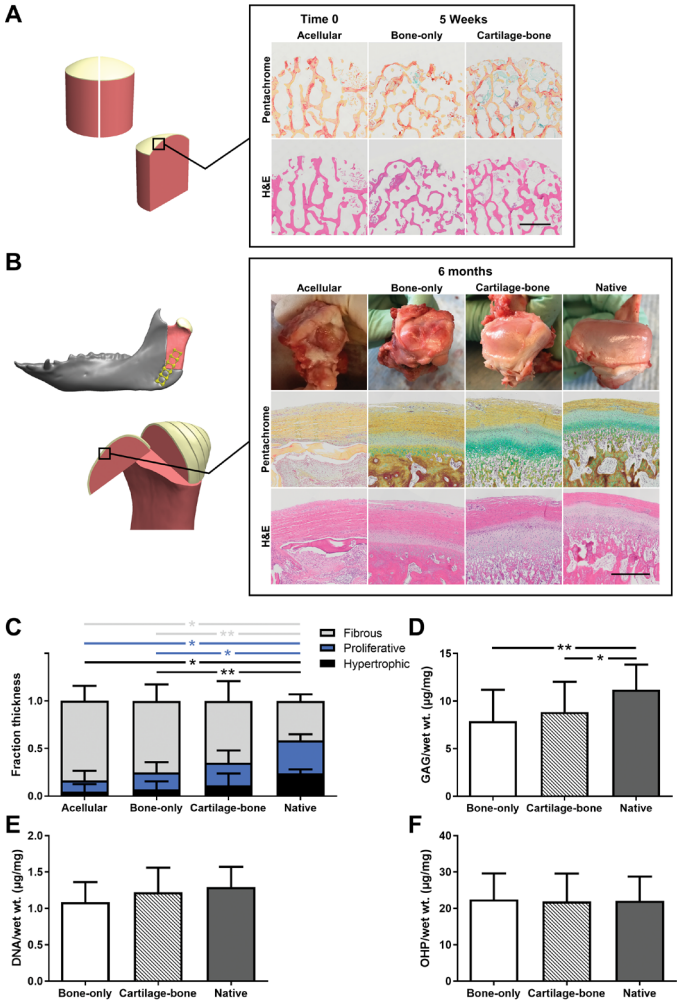

Fig. 3. Histological and biochemical properties of engineered cartilage. (**A**) Schematic and representative Movat's pentachrome and hematoxylin and eosin (H&E) staining of small constructs. Scale bar, 2 mm. (**B**) Schematic and representative photographs, Movat's pentachrome, and H&E stains of implanted and native RCUs from sagittal condylar cross sections. Scale bar, 500 μm. (**C**) Zonal distribution relative to total cartilage thickness. Data are means ± SD [$n = 3$ acellular, 8 bone-only (BO), 5 cartilage-bone (CB), and 19 native]. *P* values were determined by Kruskal-Wallis with Dunn's multiple comparison post hoc test. (**D** to **F**) GAG, DNA, and total collagen (OHP) content normalized to wet weight (wt.). Data are means ± SD ($n = 13$ BO, 11 CB, and 48 native). *P* values were determined by one-way ANOVA with Tukey-Kramer's multiple comparison post hoc test. $^{*}P < 0.05$ and $^{**}P < 0.01$.

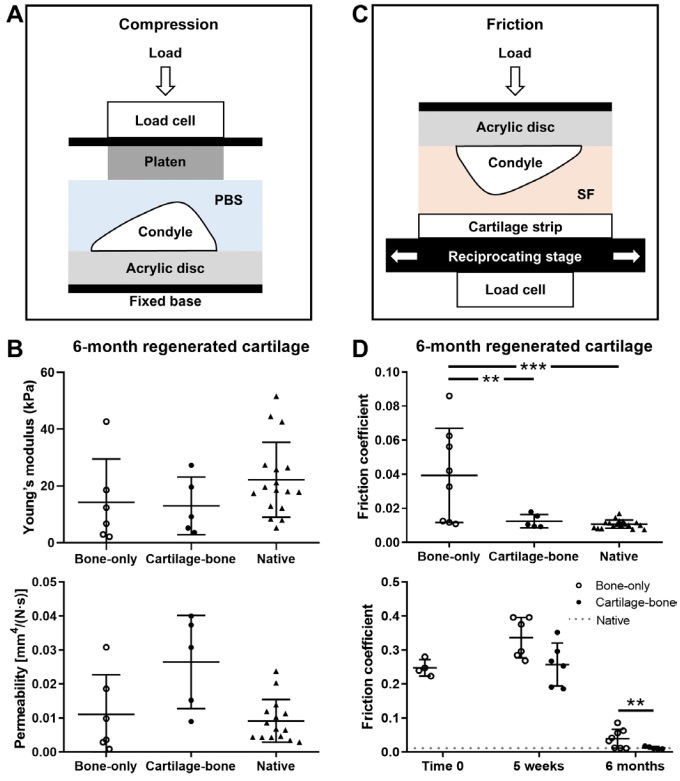

Fig. 4. Mechanical and tribological properties of engineered cartilage. Cartilage-bone RCUs achieved native-like mechanical and tribological properties after 6 months in vivo. (**A**) Schematic of uniaxial unconfined compression of intact condylar cartilage over 20 min. (**B**) Top: Young's modulus in CB, BO, and native RCUs. $n = 6$ BO, 5 CB, and 17 native. Bottom: Permeability in CB, BO, and native groups. No significant differences across groups. $n = 6$ BO, 5 CB, and 15 native. *P* values were determined by Kruskal-Wallis with Dunn's multiple comparison post hoc test. (**C**) Schematic of friction testing setup. Mean friction coefficient was calculated for a 20-min oscillating test on the intact condyle against a cartilage counterface in synovial fluid (SF). (**D**) Top: Friction coefficients of RCU condyles in CB, BO, and native cartilage samples. Bottom: Friction coefficients for CB, BO, and native RCU condyles at different time points after implantation. Data are means ± SD (RCUs: $n = 8$ BO, 5 CB, and 18 native; small constructs: $n = 4$ acellular, 6 BO, and 6 CB). *P* values were determined by one-way ANOVA with Tukey-Kramer's multiple comparison post hoc test. $^{**}P < 0.01$ and $^{***}P < 0.001$.

used in conjunction for inverse analysis and curve-fitting the raw creep data (Fig. 4A and fig. S5) (*34*). Young's modulus of the cartilage layer was measured on the peak of the entire condylar head while immersed in phosphate-buffered saline (PBS) in unconfined compression under a 0.03-N creep step load for 20 min. In a neo-Hookean ground matrix model, the Young's modulus represents the contribution of the proteoglycan constituents to compressive strength (*35*, *36*). Cartilage-bone and bone-only RCUs had similar Young's moduli and permeability values 6 months after implantation [12.97 ± 10.15 and 14.23 ± 15.26 kPa, respectively; 0.02646 ± 0.01371 and 0.01111 ± 0.01160 $mm^4/(N{\cdot}s)$], and both were comparable to the native cartilage [22.19 ± 13.19 kPa; 0.009158 ± 0.006259 $mm^4/(N{\cdot}s)$] (Fig. 4B).

The friction coefficient of each condylar surface was determined under a 4.45-N sliding load moving at 1 mm/s for 20 min against a flat cartilage counterface in a synovial fluid bath (movie S5). The entire condylar surface was measured intact, representing more physiologically faithful conditions compared to conventional testing of punch biopsy samples (Fig. 4C) (*29*, *37*, *38*). The friction coefficients measured for the native cartilage and cartilage-bone groups were comparable to those reported in the literature using similar setups (table S4). After 6 months in vivo, the friction coefficient across all groups was an order of magnitude lower than values measured after 5 weeks of in vitro culture on small tissue constructs (bone-only, 0.336 ± 0.059; cartilage-bone, 0.258 ± 0.063; Fig. 4D). These results are consistent with the thin cartilage layers on the small constructs that were observed macroscopically and histologically. The cartilage-bone RCUs achieved physiological friction coefficients with no significant difference between the engineered cartilage (0.012 ± 0.004) and native TMJ cartilage (0.011 ± 0.002)

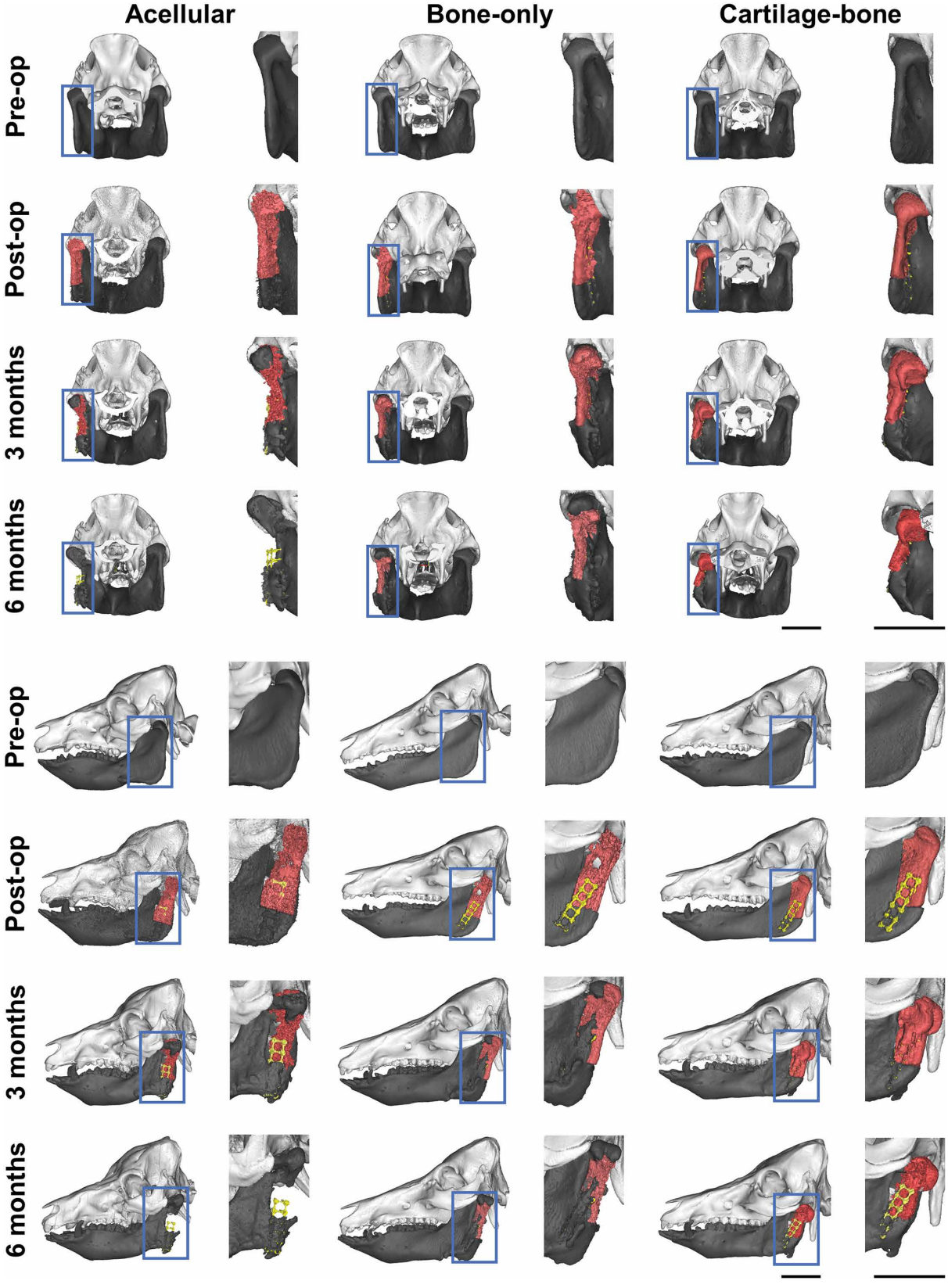

Fig. 5. Progression of ramus-condyle regeneration. Reconstructed CT scans of representative animals taken before surgery (pre-op), immediately after surgery (post-op), at 3 and 6 months. Top: Caudal view showing ramus-condyle height on implant versus native side of the jaw. Bottom: Lateral view showing fixation and integration of implanted RCU with the surrounding native bone. Boxed regions are shown at higher magnification on the right in each column.

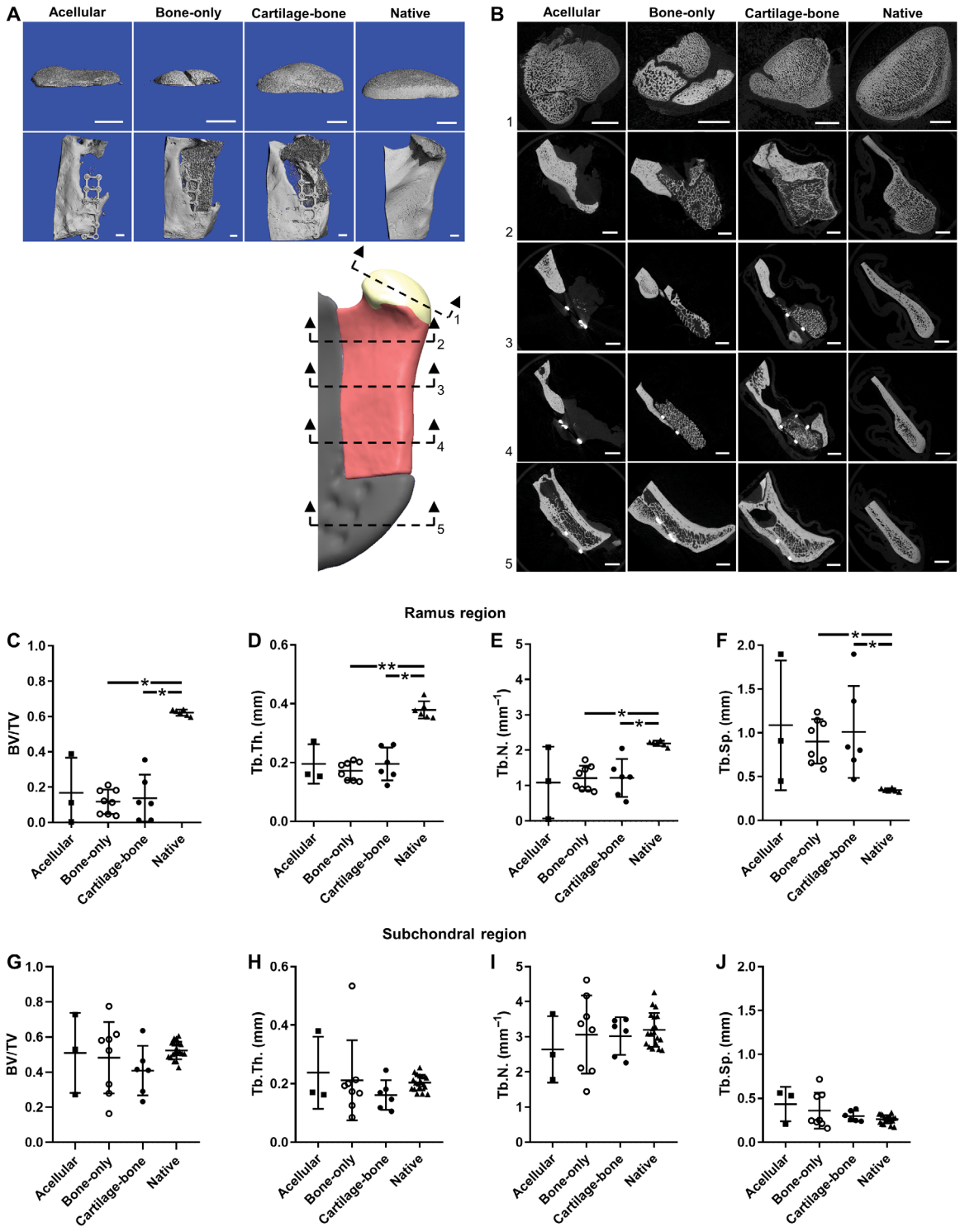

Fig. 6. Morphology and structure of engineered bone. (**A**) Reconstructed μCT scans of representative samples. Top: Representative condyles in acellular, BO, CB, and native samples. Bottom: Representative rami samples. Scale bars, 5 mm. (**B**) Cross-sectional μCT images. Scale bars, 5 mm. (**C** to **F**) μCT quantification of rami regions above the metal fixation plate. Bone volume over total volume (BV/TV), trabecular thickness (Tb.Th.), trabecular number (Tb.N.), and trabecular spacing (Tb.Sp.) of engineered and native RCUs. Data are means ± SD ($n = 3$ acellular, 8 BO, 6 CB, and 6 native). (**G** to **J**) μCT quantification of the subchondral bone. BV/TV, Tb.Th., Tb.N., and Tb.Sp. in engineered and native samples. Data are means ± SD ($n = 3$ acellular, 8 BO, 6 CB, and 19 native). *P* values were determined by Kruskal-Wallis with Dunn's multiple comparison post hoc test. $^{*}P < 0.05$ and $^{**}P < 0.01$.

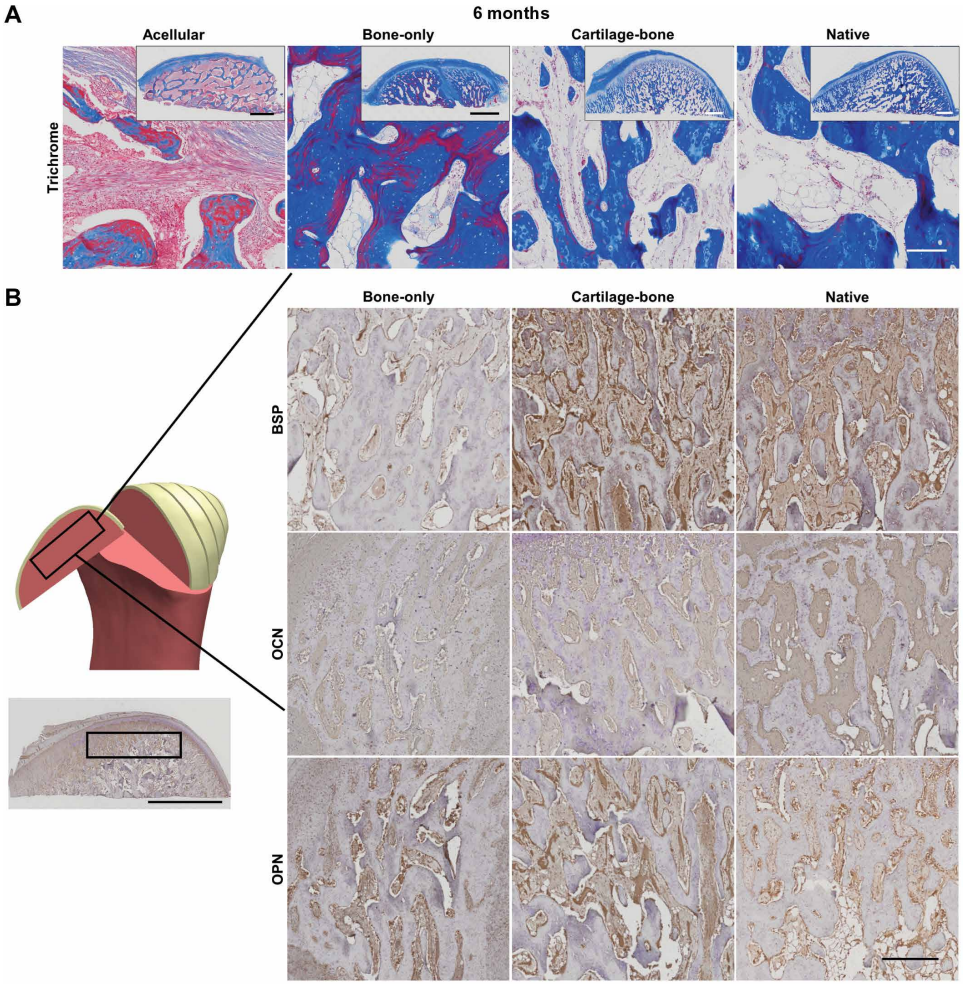

Fig. 7. Histological properties of engineered subchondral bone. (**A**) Representative Masson's trichrome staining in sagittal subchondral cross sections of acellular, BO, CB, and native samples. Scale bars, 200-μm high magnification and 2-mm low magnification. (**B**) Schematic and representative immunohistochemistry staining for common bone markers' bone sialoprotein (BSP), osteocalcin (OCN), and osteopontin (OPN). Images are taken from the indicated area on a low magnification image of a native sample. Scale bars, 500-μm high magnification and 5-mm low magnification.

(Fig. 4C). In comparison, the bone-only RCUs (0.039 ± 0.028) had significantly higher friction coefficients than either the cartilage-bone ($P < 0.01$) or native ($P < 0.001$) groups (Fig. 4D and fig. S6).

Engineered bone exhibits comparable features in cartilage-bone and bone-only RCUs but not in acellular controls

After 6 months in vivo, the engineered bone throughout the ramus region in cartilage-bone RCUs was comparable to the engineered bone in bone-only RCUs. The whole-jaw CT scans taken before surgery, immediately after surgery, 3 months after surgery, and 6 months after surgery showed that the cartilage-bone and bone-only groups had similar bone tissue maintenance and structural integrity. Nearly all cartilage-bone and bone-only RCUs had considerable bone growth in the transverse plane along the thinnest dimension of the ramus, and integration between the implanted graft and native bone was incomplete and largely supported by fibrous tissue. In contrast, there was total or substantial resorption in the ramus region in samples from the acellular control group, leaving a large cap with no mineralized bone underneath (Fig. 5).

In the ramus regions, more distal from the condyle, three-dimensional (3D) μCT reconstructions confirmed similar microstructure and mineral distribution in the engineered bone in the cartilage-bone and bone-only groups 6 months after implantation and greater bone development compared to the acellular group (Fig. 6A). μCT cross sections throughout the ramus matched macroscopic observations and CT data that showed similar bone morphology in the ramus regions of the cartilage-bone and bone-only groups, contrasted with substantial bone loss in the acellular controls (Fig. 6B). μCT quantification (bone volume normalized by total volume, trabecular thickness, trabecular number, and trabecular spacing) of the ramus regions also confirmed that the cellularized RCUs performed similarly, although none matched native bone values (Fig. 6, C to F). One of three acellular scaffolds performed better and led to high variance in the group. The comparable features achieved in the ramus regions of the cartilage-bone and bone-only RCUs indicate that the added complexity of engineering the cartilage-bone RCUs did not compromise the previously established quality of engineered bone in large anatomical RCUs (*19*).

In the condylar region, 3D and cross-sectional μCT images indicated that native-like bone was regenerated in the cartilage-bone group in the subchondral region after 6 months in vivo. The health and morphology of the subchondral bone is known to contribute to cartilage health and load sharing (*39*, *40*). In the bone-only and acellular groups, there was often incomplete remodeling with noticeable fissures and inhomogeneous trabecular size and spacing, whereas the cartilage-bone RCUs recapitulated native-like appearance (Fig. 6, A and B). μCT quantification confirmed that the subchondral bone of the cartilage-bone group was similar to native tissue, and there was less intersample variability compared to the bone-only and acellular groups (Fig. 6, G to J), although there were no statistically significant differences with respect to bone volume and trabecular morphology between groups. Masson's trichrome staining of the subchondral bone also showed a positive progression from osteoid-heavy, immature bone tissue in the acellular implants, to more mature bone matrix in the cartilage-bone RCUs after 6 months in vivo (Fig. 7A). Stains for known osteogenic markers in the RCUs further confirmed the native-like morphology of the engineered subchondral bone. Compared to native samples, stains from the cartilage-bone and bone-only groups were similarly positive in osteocalcin (OCN) and osteopontin (OPN). For bone sialoprotein (BSP), cartilage-bone and native samples appeared to stain similarly, whereas bone-only samples stained weaker (Fig. 7B).

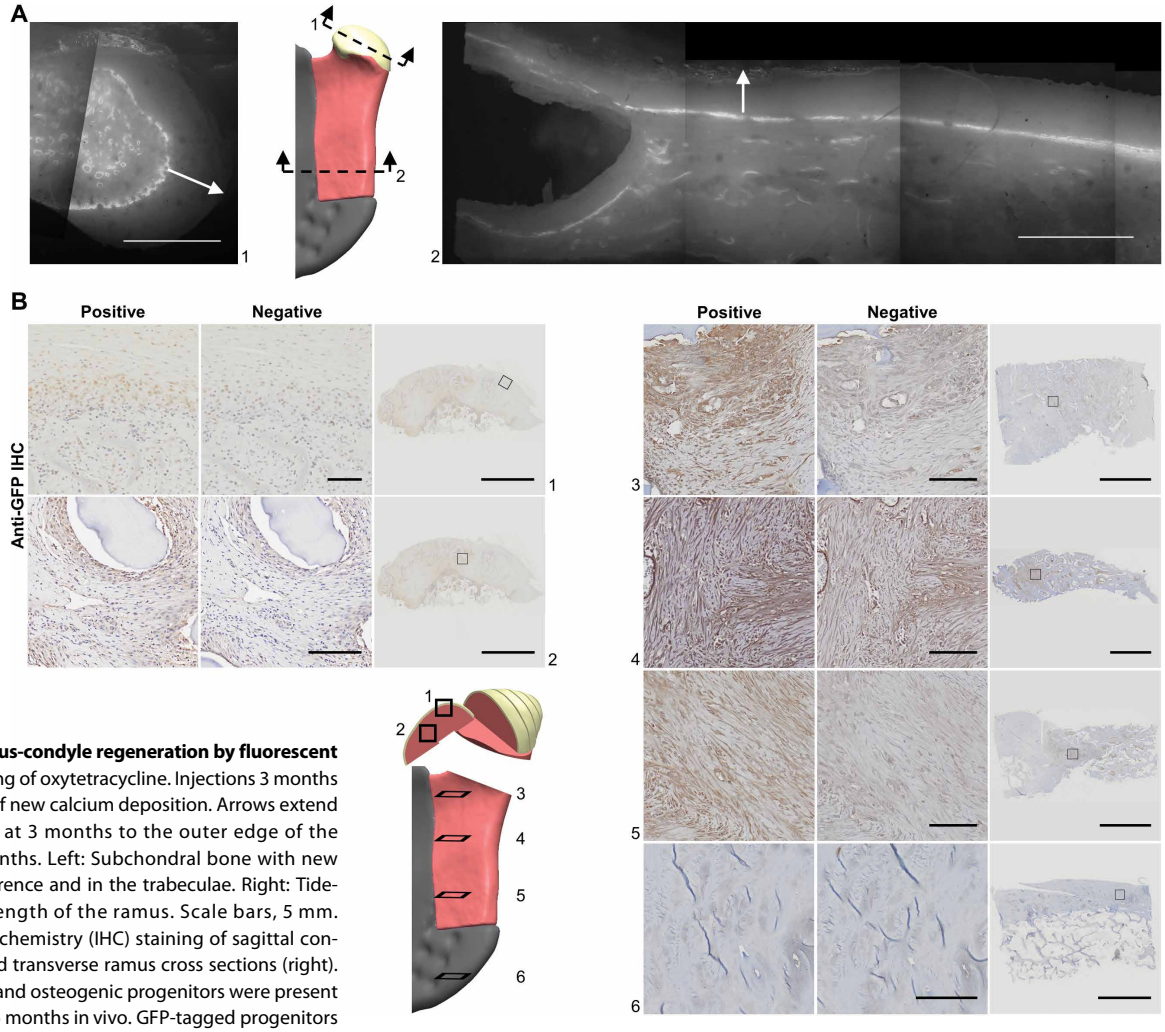

Fig. 8. Visualization of ramus-condyle regeneration by fluorescent tags. (**A**) Fluorescent imaging of oxytetracycline. Injections 3 months after surgery marked sites of new calcium deposition. Arrows extend from the deposition sites at 3 months to the outer edge of the explanted sample at 6 months. Left: Subchondral bone with new growth along the circumference and in the trabeculae. Right: Tidemark pattern along the length of the ramus. Scale bars, 5 mm. (**B**) Anti-GFP immunohistochemistry (IHC) staining of sagittal condyle cross sections (left) and transverse ramus cross sections (right). GFP-tagged chondrogenic and osteogenic progenitors were present throughout the graft after 6 months in vivo. GFP-tagged progenitors were not located in native tissue surrounding the graft. Negative immunohistochemistry is shown to account for nonspecific background staining, with darker brown staining in positive immunohistochemistry panels indicating GFP-positive cells. Scale bars, 100-μm high magnification and 5-mm low magnification.

Cell labeling indicates that implanted cells are present in the regenerating tissues

Oxytetracycline injections at 3 months after surgery marked patterns of new bone deposition that occurred between 3 and 6 months. Within the subchondral bone, there was positive signal along the radial circumference and in the trabeculae pores, perhaps indicating new bone deposition both along the periphery and in the internal structure. In the ramus, the oxytetracycline revealed a tidemark (interface between calcified and noncalcified tissue) running down the transverse length (Fig. 8A).

To investigate the role of the implanted ASCs in the regenerative process, groups of RCUs contained green fluorescent protein (GFP)–tagged chondrogenic progenitors or GFP-tagged osteogenic progenitors (table S5). It was difficult to directly visualize cell fluorescence within the excised tissues; however, we located labeled cells via positive anti-GFP immunohistochemical staining in both cartilage-bone and bone-only groups after 6 months in vivo. GFP-tagged chondrogenic progenitors were found throughout the condylar region of the RCU, both within the cartilage surface where they were first seeded and extending into the subchondral bone. GFP-tagged osteogenic progenitors were found throughout the ramus where they were initially seeded in the RCU but also further up into the remodeled subchondral bone, suggesting that these cells and their progeny played a role in the regeneration process, at least near the condyle (Fig. 8B). GFP-tagged cells were seen across the graft volume but not in the native bone surrounding the implanted RCU, indicating that these cells did not migrate out of the graft into the surrounding bone.

DISCUSSION

We engineered human-sized, anatomically precise cartilage-bone grafts representing an entire RCU for repairing the lower jaw, by bioreactor culture of autologous ASCs in decellularized bone scaffolds. In a clinical scale animal model (Yucatan minipig), we demonstrated the utility of these grafts for the functional repair of the ramus-condyle region in healthy animals. Using CT scans of each animal (to fabricate the scaffold and the matching bioreactor chamber) and a minimally invasive adipose tissue harvest (to generate therapeutic cells), each graft was prepared in an animal-specific manner. Safety and biocompatibility were confirmed by maintenance or increase in animal weight, as well as by normal ranges of blood counts and serum chemistry values measured across 6 months.

To mimic the envisioned centralized production of the grafts and their distribution to hospitals, the grafts were cultured at one location (New York, NY) and implanted at another, distant location (Baton Rouge, LA). For further clinical reference, the implantations were conducted by an expert maxillofacial surgeon, using standard clinical protocols and tools for TMJ surgery (fig. S7).

The advantages of implanting the RCU containing a cartilage layer integrated with the underlying condyle bone as compared to the bone-only and acellular grafts were evidenced by the superior appearance, morphology, biochemical content, and mechanical properties of the cartilage-bone grafts after 6 months of implantation. This achieved native-like cartilage formation in the reconstruction of a large, load-bearing craniofacial defect.

Toward the treatment of large cartilage-bone defects using tissue engineering approaches, early work focused on establishing the optimal environment to support regeneration. The use of the in vivo environment as a bioreactor helped inspire designs of more advanced in vitro bioreactors (*41*–*43*). For craniofacial tissue engineering in particular, initial efforts targeted the repair of small bone-only defects in non–load-bearing regions of the skull (*44*–*47*). More recent work addressed large defects in load-bearing regions of the mandible but primarily emphasized bone formation and integration (*17*, *19*). Some studies have attempted to incorporate the cartilage with the bone but have primarily performed so in vitro with decellularized bone matrix (*21*, *22*). Functional repair of ramus-condyle defects relies on the presence of both tissue types—cartilage and bone. Our study bridges this gap by incorporating a cartilage layer on top of a large living bone graft, thereby taking an important step toward clinical translation of engineered grafts. After 6 months in vivo, the resulting cartilage-bone RCUs recapitulated key native-like features within the regenerated cartilage. Using the bone-only RCUs and native contralateral tissues as benchmarks, the cartilage-bone RCUs produced cartilage with better gross appearance, zonal distribution, and expression of key markers. In particular, the cartilage of the cartilage-bone and native samples contained mostly collagen II, whereas the bone-only samples predominantly featured collagen I. This corroborates the more fibrocartilaginous profile of the cartilage in the bone-only RCUs and could explain why the total measured collagen was similar amongst the groups. Although biochemical analyses of small local biopsies indicated no significant difference in GAG content between cartilage-bone and bone-only RCUs, comprehensive pentachrome staining revealed the spatial distribution of GAGs throughout the entire sagittal condylar plane with more native-like zonal organization in the cartilage-bone group. Future studies should perform additional quantitative enzyme-linked immunosorbent assay analyses for collagen and GAG subtypes.

The cartilage-bone RCUs successfully restored functionality of the jaw, as indicated by the native-like mechanical properties of the cartilage layer 6 months after implantation. Nondestructive mechanical tests were conducted on the entire fresh condylar head, to mimic physiological loading conditions as closely as possible. Because measured values can be affected by the testing setup and parameters, we benchmarked our values using the native contralateral side in addition to the literature data on native porcine TMJ. This approach allowed rigorous mechanical and tribological testing of large tissue-engineered condyles.

The 6-month postimplantation cartilage-bone RCUs achieved an average friction coefficient (0.012) that closely matched that of native cartilage (0.011), with both values being significantly lower than the coefficients achieved by the bone-only RCUs (0.039). The measured Young's moduli for the cartilage on the cartilage-bone RCUs also were in the range of native tissues, and similar to the moduli for bone-only RCUs, presumably because the Young's modulus represents a bulk measurement of cartilage properties that does not reflect the differences in its zonal organization between the groups. Likewise, there was no difference in total collagen content between groups; however, the cartilage-bone grafts and native tissues contained mostly collagen II, whereas bone-only tissues were dominated by collagen I. The friction coefficient may be a more realistic indicator of the properties of the cartilage layer, because it is largely determined by the superficial layer of the cartilage. Cartilage-bone RCUs had low, native-like friction coefficients unlike their bone-only counterparts. Bite force measurements, mastication imaging, and synovial fluid and TMJ disc analyses could provide additional insight into the quality and function of the regenerated cartilage.

Previous work demonstrated that the in vitro formation of the cartilage is markedly facilitated by the underlying decellularized bone matrix (*21*). Clinically, it is known that the subchondral bone plays a role in the initiation and progression of cartilage damage (*39*, *40*, *48*). We were interested in the effects of the cartilage layer on the formation of the subchondral bone. The subchondral bone in the 6-month postimplantation cartilage-bone RCUs recapitulated the mature bone matrix and trabecular distribution of the native tissue, in contrast to the more variable and osteoid-heavy immature bone matrix of the bone-only and acellular RCUs. The key marker BSP appeared more highly expressed in the subchondral bone of cartilage-bone RCUs compared to bone-only RCUs, whereas OCN and OPN were similarly stained. In the more distant ramus, the bone quality was less affected by the cartilage layer and remained comparable to the bone-only group. Acellular RCUs showed greater bone resorption 6 months after implantation, although some resorption was observed in both cartilage-bone and bone-only RCUs. Bone resorption rates are known to be a function of postoperative immobilization (*49*), and although the animals in this study were immediately allowed to return to normal function, additional studies are needed to determine best practices for improved regenerative outcomes. Three-point bending tests for peak and equilibrium flexural modulus and force could be used for future mechanical testing of the bone (*19*).

In addition to demonstrating safe and effective repair of the large defects in the lower jaw using engineered RCUs, our objective was to investigate the progression of the regenerative processes and the respective contributions of the living cartilage and bone regions. We hypothesized that our cartilage-bone RCU would serve as a template for remodeling and regeneration, rather than a direct replacement of the native tissue. To this end, we compared tissue properties before implantation (after 5 weeks of bioreactor culture) and after 6 months in vivo. The inclusion of a cartilage precursor positively contributed to tissue regeneration in vivo, as seen by the more native-like phenotype of the cartilage in the cartilage-bone RCUs compared to the bone-only RCUs. Consistently, the small difference in cartilage friction coefficients between the cartilage-bone group and bone group at the end of in vitro culture markedly increased by 6 months of implantation, with cartilage-bone group reaching the frictionless behavior of native tissue samples. The GFP-positive cartilage or bone precursor cells initially seeded in grafts that we were able to locate after 6 months of implantation indicated that the implanted cells had lasting contributions to regeneration.

Another fluorescent tag, oxytetracycline, allowed us to identify the areas of calcium deposition within implanted RCUs in both the subchondral and ramus regions of the bone and indicated that further remodeling took place after the 3-month mark. Together, these data provided two important insights: (i) the majority of tissue remodeling and regeneration occurred in vivo and (ii) the progression and outcomes of tissue regeneration depended on the properties of the engineered graft. The cartilage-bone RCUs served as the most effective regeneration templates, resulting in the best structural and functional tissue properties.

A limitation of this study is the lack of histomorphological and biomechanical analyses at additional time points to better understand the regenerative processes that occur in vivo. Studies over longer periods of time would lead to more detailed understanding of the remodeling of engineered RCUs. Future studies should not only focus on more temporal analyses but also make use of alternative labeling methods for longitudinal cell and extracellular matrix tracking (*50*). In addition, it has been shown in many tissue types that mechanical conditioning can help create more mature tissues in vitro (*51*–*53*). Because healthy bone remodeling depends on appropriate mechanical stimuli (*54*), a more advanced bioreactor should have both loading and perfusion capabilities.

The engineered bone in this study was composed of decellularized bovine bone matrix and osteogenic porcine cells. We hypothesized that the inclusion of additional cell types such as osteoclasts, endothelial, and stromal cells would further improve the integrity of our engineered bone. From a disease modeling perspective, it would also be advantageous to develop a model incorporating more cell types. Particularly in the TMJ, vascularization and chondrocyte-osteoblast transdifferentiation were recently reported to play a role in osteoarthritis and other pathologies (*55*). Our study was conducted in healthy animals, and future studies are needed to evaluate the graft performance in more challenging unhealthy joint environments. Although age was randomly distributed between experimental groups, the animals in our study were relatively young overall, between 13 and 23 months at the time of graft implantation, and all animals were male. Future studies are needed to understand the potential contributions of ASC donor and engineered graft recipient ages to regenerative outcomes and to investigate any sex-based differences. Last, inclusion of the adjacent tissues such as soft connective tissues and the TMJ disc (*56*, *57*) could further extend the functional integration of engineered RCUs with the host.

The animals in this study were immediately allowed to return to a solid diet, and the positive performance of our implanted grafts may suggest limiting the duration of jaw immobilization in patients after an analogous procedure. The 11-week preparation and in vitro culture period is compatible with the timeline of two-stage maxillofacial reconstruction, which is widely used for many clinical indications, from cancer surgery to traumatic injury. The time between the first operation (damaged tissue resection and space maintainer placement) and the second operation (graft reconstruction) usually spans several months, allowing ample time to prepare and culture patient-tailored living autologous grafts (*58*, *59*). The time limiting step in our current protocol is the expansion of cells to usable numbers. We chose to conduct this initial study using autologous cells for rigor of experimental design. Mesenchymal stromal/stem cells have substantial immune privilege and can be transplanted between human leukocyte antigen–incompatible patients without adverse response (*60*), an option that needs to be validated, as it would lead to an off-the-shelf therapy. Overall, this study resulted in a promising approach to large-scale joint reconstruction using viable tissues and opened several avenues of investigation.

MATERIALS AND METHODS

Study design

Our objective was to engineer autologous, living, anatomically correct cartilage-bone craniofacial grafts for implantation using ASCs, native bone matrix scaffolds, image-guided fabrication methods, and dual perfusion bioreactors with the cartilage and bone regions independently supplied by their optimal media and regulatory signals. We hypothesized that immature cartilage and bone tissues formed in vitro would serve as effective templates for functional tissue development, maturation, and integration in vivo. Bioengineered grafts were investigated for their capacity to regenerate the RCU to a native-like state during a 6-month period of implantation in Yucatan minipigs. To recapitulate the envisioned clinical application of bioengineered grafts that will be prepared at centralized locations and shipped to hospitals for implantation, the grafts were cultured in our laboratory in New York City and implanted into animals residing in Baton Rouge, LA (a 10-hour distance door to door).

Three groups of bioengineered grafts were investigated: (i) cartilage-bone RCUs (the main experimental group), (ii) bone-only RCUs (to assess the regenerative ability of bone and any spontaneous generation of cartilage), and (iii) acellular scaffolds (to assess the role of exogenous cells in regeneration); data for the condylectomy (no treatment group) are available from our previous study in the same animal model (*19*). Selection of animals into the experimental groups was randomized. The cells used to seed the scaffolds were derived from a small fat sample (100 ml) taken from each animal (autologous cells). The scaffold and bioreactor chamber for each animal were specifically made using image-guided fabrication to fit the exact geometry of that animal's defect. Tissue outcomes included histology, immunostaining, mechanical testing, CT, and μCT imaging.

To understand the regenerative processes driven by our grafts in vivo, we fluorescently tagged the chondrogenic and osteogenic progenitor cells in some of our grafts, performed CT imaging at multiple time points, and used oxytetracycline to visualize new bone formation. To understand the maturation of our tissues during in vitro culture, we also studied miniaturized, cylindrical cartilage-bone constructs in the same experimental groups (cartilage-bone, bone, and acellular scaffold) and using the same methods as for the clinically sized grafts. These smaller constructs had thicknesses corresponding to the critical distances for nutrient transport, cell migration, and mechanotransduction in the larger anatomical grafts and were designed to correspond to a core taken from the middle of the RCU condyle. To eliminate the potential biological differences in regenerative capacity of the cells, we pooled the ASCs sourced from $n = 7$ animals. The small constructs were grown in bioreactors using the same culture media and under the same local velocities as the anatomical grafts during perfusion culture. The assays for evaluating tissue outcomes were also the same as for the anatomical grafts.

The implantation studies were conducted using 20 skeletally mature male Yucatan minipigs between 13 and 23 months old, weighing 58.7 ± 11.5 kg (table S1). The sample size of $n = 5$ or greater per group was determined using power analysis, with an SD of 20%

(based on the 10 to 20% SD observed in cartilage friction coefficients from our previous in vitro cartilage work) (*21*), a power of 90%, a difference to detect 50% of the mean average, and an α value of 0.05. The sample size of $n = 5$ or greater per group for in vitro constructs was determined similarly. Specific information about sample size, data collection, and inclusion and exclusion criteria are provided for each experimental stage.

Of the 20 animals, 19 underwent the procedure until the 6-month end point without apparent distress. One animal was euthanized early (1 month after surgery) after implant displacement due to the snapping of the fixation plate. Another animal developed infection as determined from inspection by an expert maxillofacial surgeon. Although there was no frank purulence, the gross appearance of the tissue was necrotic and indicative of a chronic infection. One animal lacked the TMJ disc and synovial fluid. After exclusion of these three animals, we analyzed the remaining 17 implanted RCUs (cartilage-bone, $n = 6$; bone-only, $n = 8$; acellular controls, $n = 3$) (table S5), along with the 19 native contralateral RCUs.

Perfusion bioreactor design and operation

The perfusion bioreactors were developed starting from a previous bioreactor system that was used to generate anatomical pieces of the tissue-engineered bone (*19*). Additional fluidic routing conduits were designed to perfuse chondrogenic medium along the condylar surface, without mixing with the osteogenic medium introduced into the bone region, using a soft, disposable polydimethylsiloxane (PDMS; Dow Corning) manifold assembled around the graft in three sections. Two sections distributed the flow of osteogenic media throughout the graft, one at the inlet side and one at the outlet side. These two sections were created with channels for bone perfusion whose size, placement, and number were designed to provide an optimal flow velocity (800 μm/s) throughout the graft (*19*, *27*). The design objective was to provide adequate mass perfusion along the perfusion paths ranging from 5 to 7 mm (thickness of the ramus) to 25 mm (at the condylar head). The third section of the manifold transported the chondrogenic media, which was routed along flow channels from inlet to outlet on the surface of the condyle. The channels were about 0.75 mm in height, 1.0 mm in width, and spaced 2.0 mm center to center and were aligned in parallel to the sagittal plane. The chondrogenic cells at the surface of the graft were shielded from fluidic shear stress with a porous hydrophobic membrane (1-μm pores, Sterlitech Corp.). The three PDMS manifolds were sealed against the graft by an external shell machined from polycarbonate. Peristaltic tubing from the inlet and outlet ports in each section of the bioreactor was connected to a pump and reservoir for recirculating flow.

Cultivation of the cartilage layer

The cartilaginous layer was generated from condensed mesenchymal cell bodies (CMBs) using our previously established protocol (*21*). Passage 5 ASCs were suspended in chondrogenic medium [high-glucose Dulbecco's modified Eagle medium (DMEM; Gibco) supplemented with TGF-β3 (10 ng/ml; PeproTech), dexamethasone (100 nM; Sigma-Aldrich), ascorbic acid 2-phosphate (50 μg/ml; Sigma-Aldrich), sodium pyruvate (100 μg/ml; Corning), proline (40 μg/ml; Sigma-Aldrich), 1% insulin, transferrin, sodium selenite (Corning) mix, and 1% penicillin/streptomycin (P/S; Gibco)]. Each CMB was formed using 2.5×10^5 cells/ml based on previous experiments, demonstrating the formation of compact spherical bodies measuring 1 mm in diameter (*21*). Cell suspension was aliquoted into deep round-bottom 96-well plates at 1 ml per well and centrifuged at 250*g* for 5 min, and the CMBs were allowed to self-assemble over 3 days in the incubator at 37°C, 5% (v/v) CO_2 with daily media changes.

The cartilage region covering the articulating surface of the condyle was sized to 1 mm in thickness, corresponding to 800 CMBs per anatomical scaffold and 120 CMBs per small scaffold. The scaffold condylar surface areas determined by the SOLIDWORKS software were 4 to 5 cm^2 for the anatomical scaffolds and 0.70 cm^2 for the small scaffolds. The CMBs were placed onto the polycarbonate membrane cut to match the condylar surface, in the void of the condylar PDMS block, and the decellularized scaffold was pressed onto the CMB layer.

The CMB layer was allowed 1 day to attach to the scaffold under static culture conditions, with the bioreactor oriented with the condylar end facedown. Chondrogenic media were perfused for 5 weeks over the condylar surface at a flow rate of 1 ml/min, separated from direct contact with the CMB layer by the polycarbonate track etch (PCTE) membrane to reduce shear stress. Culture medium was changed twice per week. The total culture time was selected on the basis of preliminary studies for the CMBs to form a cartilage layer integrated with the underlying scaffold. Osteogenic cells were introduced to the graft 2 weeks after the initial seeding of the CMB layer, by which time a compact cartilage layer has been formed.

Cultivation of bone region

Passage 5 ASCs were suspended in osteogenic medium [low-glucose DMEM (Gibco) supplemented with 10% fetal bovine serum (Corning), 1% P/S, 10 mM sodium β-glycerophosphate (Sigma-Aldrich), 100 nM dexamethasone, and ascorbic acid 2-phosphate (50 μg/ml)]. The scaffold volumes as determined by the SOLIDWORKS software were in the range of 9 to 15 cm^3 for the anatomical scaffolds and 0.53 cm^3 for the small scaffolds. Cell suspension (10^7 cells/cm^3) was infused into the bioreactor chamber, using 12-ml volume for the anatomical scaffold and 630-μl volume for the small scaffold. The cells were allowed 3 hours to attach to the scaffold under static culture conditions, and the bioreactor was flipped every 30 min to facilitate spatially uniform attachment throughout the scaffold volume. Osteogenic media were perfused through the construct for 3 days at 10% of the calculated optimal flow rate (80 μm/s) and for an additional 3 weeks at the set optimal flow rate (800 μm/s), with medium changes twice per week. The culture time was selected on the basis that ASCs highly express osteogenic markers after 3 weeks of in vitro differentiation.

Animal implantation

The animal implantation study was conducted at the Louisiana State University School of Veterinary Medicine under an approved Institutional Animal Care and Use Committee protocol (14-077). A total of 20 skeletally mature Yucatan minipigs (Lonestar Laboratory Swine) were randomly assigned to three treatment groups: (i) acellular scaffold implantation ($n = 3$), (ii) engineered bone implantation ($n = 9$), and (iii) engineered cartilage and bone implantation ($n = 8$). Skull CT scans (GE LightSpeed 16; 120-kV peaks and 635-mm resolution) were performed on all animals at the time of adipose harvest, 2 to 3 months before facial surgery, to provide the scaffold fabrication data. Each animal was investigated in a longitudinal study with data collection up to 6 months after implantation.

For each animal, we used its reconstructed 3D CT images (described in the "Scaffold fabrication" section in Supplementary Materials and Methods) to select the left TMJ RCU, measuring about 3 cm along the dorsal plane by 6 cm along the transverse plane, as the region for defect creation and reconstruction. In addition, the Digital Imaging and Communications in Medicine dataset obtained from the preoperative CT scan was used to perform virtual surgical planning (3D Systems Inc.). Through an online meeting between the maxillofacial surgeon and the 3D Systems Inc. engineer, the resection was mapped out on the reconstructed CT scan and surgical cutting guides were manufactured.

The grafts were grown in three separate experiments, with randomized division of animals into experimental groups. Grafts from the same experiment were implanted on consecutive days, with two to three surgeries performed per day. The surgical procedure was designed by an expert maxillofacial surgeon to closely mimic the current clinical procedure in human patients.

After 12 hours of fasting, animals were sedated with ketamine (3 mg/kg), tiletamine (2 mg/kg), and xylazine (3 mg/kg), administered intramuscularly. Anesthesia was then induced with 5% isoflurane (MWI Veterinary Supply) in 100% oxygen (1.5 liters/min) via facial mask. The animals were intubated with a cuffed Murphy's endotracheal tube (7 to 9 mm in internal diameter), and anesthesia was maintained at a vaporizer setting of 1.5% isoflurane and oxygen flow rate of 1 to 2 liters/min in a closed circular system. The left side of the face was aseptically prepared with alternating chlorhexidine and isopropyl alcohol scrubs and draped to isolate the surgical field.

The planned retromandibular and submandibular incision was then marked about 1 to 2 cm below the inferior border of the mandible. After incising through the skin and subcutaneous tissue, dissection continued to the inferior and posterior border of the mandible. The pterygoid-masseteric muscle sling was then sharply incised to expose the entire lateral surface of the ramus and condyle. A retractor was placed in the sigmoid notch to reflect the flap superiorly. The medial pterygoid muscle was also elevated.

The surgical cutting guide was then placed and secured with two 1.7-mm screws of 8 to 10 mm in length (Stryker Inc.). A reciprocating saw with saline irrigation was then used to create a vertical osteotomy from the sigmoid notch that was joined to a horizontal osteotomy. The ramus/condyle unit was then dissected free from its attachments and delivered.

The animal-specific graft was inserted and rigidly fixated with either a box plate (6 screws each side, 12 total) or two straight plates (7 screws each plate, 14 total) with 2.0-mm diameter screws (Stryker Inc.) (fig. S7). The incision was subsequently closed in layers using standard technique. A sterile dressing was applied, and an immediate postoperative CT scan was performed before extubation. Animals were treated for post-operation pain relief with buprenorphine (0.03 mg/kg) intramuscularly every 6 hours for 24 hours after extubation and phenylbutazone (5 mg/kg) every 24 hours for 3 days.

Mechanical testing

Frictional properties were determined by placing the condyle in contact against a cartilage counterface under 4.45-N load and prescribing sliding motion over a 5-mm wear track (1 mm/s, 120 cycles). Tangential and normal forces to the articular surface were recorded and used to determine the friction coefficient, which was then averaged and reported over each cycle. After frictional testing and sufficient relaxation, unconfined compression creep tests were performed under a 0.03-N load for a duration of 20 min. Creep testing was chosen because cartilage thicknesses were unknown before mechanical testing and strains could not be prescribed. Sample-specific geometry was obtained from laser scans and used to develop FEBio finite element models replicating the unconfined compression creep tests (total thickness: bone-only, 0.579 ± 0.243; cartilage-bone, 0.622 ± 0.331; native, 0.422 ± 0.0799 mm; final contact areas: bone-only, 4.000 ± 0.255; cartilage-bone, 7.354 ± 4.169; native, 4.167 ± 1.752 mm^2) (data file S1). The data from those tests were used in the models to extract Young's modulus E and hydraulic permeability k for each sample. The final engineering strains were calculated from thicknesses as determined by histology and displacement data as measured by the proportional-integral-derivative controller (bone-only, 0.246 ± 0.140; cartilage-bone, 0.268 ± 0.148; native, 0.182 ± 0.051) (data file S1). Additional details are provided in Supplementary Materials and Methods.

Statistical analysis

Statistical analysis was conducted using GraphPad Prism 8 software (GraphPad Software Inc.). Data for cartilage thickness, biochemical content, friction coefficient, creep compression parameters, and μCT bone quantification were checked for whether they fit Gaussian distributions using the Shapiro-Wilk normality test. When normality was confirmed, statistical analysis was carried out by one-way analysis of variance (ANOVA) test and post hoc Tukey-Kramer's comparison test to compare means between groups (biochemical content, Young's modulus, and friction coefficient). When normality was not confirmed or when sample size was <4, statistical analysis was carried out by nonparametric Kruskal-Wallis test and post hoc Dunn's multiple comparison test to compare the means between groups (cartilage thickness, permeability, and μCT bone quantification). Native data, which were expected to be normally distributed, were checked for outliers using the robust regression and outlier removal method and a Q coefficient of 1% to limit the false discovery rate (*61*). Specific information about sample size, data collection, and inclusion and exclusion details are provided in the context of each experimental stage. Data were calculated as means ± SD. $P < 0.05$ was considered significant.

SUPPLEMENTARY MATERIALS

stm.sciencemag.org/cgi/content/full/12/565/eabb6683/DC1

Materials and Methods

Fig. S1. Cartilage-bone perfusion bioreactor design.

Fig. S2. Graft excision after 6 months of implantation.

Fig. S3. Morphology and composition of the engineered cartilage.

Fig. S4. Additional histological properties of the engineered cartilage.

Fig. S5. Creep compression of the engineered cartilage.

Fig. S6. Tribological properties of the engineered cartilage.

Fig. S7. RCU fixation during surgery.

Table S1. Animal ages at surgery and weights before surgery, after 3 months, and after 6 months.

Table S2. Complete blood counts after surgery, 3 months, and 6 months.

Table S3. Metabolic panels after surgery, 3 months, and 6 months.

Table S4. Published values on friction and modulus data for porcine TMJ.

Table S5. Experimental groups.

Movie S1. Computational simulated flow through RCU bioreactor.

Movie S2. Filling of ramus-condyle scaffold and bioreactor with medium.

Movie S3. Computational simulated flow through small construct bioreactor.

Movie S4. Filling of small scaffold and bioreactor with medium.

Movie S5. Cartilage friction testing.

Data file S1. Primary data for cartilage thicknesses, biochemistry, creep compression, friction, and μCT.

References (*62*–*76*)

View/request a protocol for this paper from *Bio-protocol*.

REFERENCES AND NOTES

1. National Institute of Dental and Craniofacial Research, "TMJ (Temporomandibular Joint and Muscle Disorders) causes, symptoms, diagnosis, treatment" (2018); www.nidcr.nih.gov/health-info/tmj/more-info.
2. M. J. Troulis, F. T. Tayebaty, M. Papadaki, W. B. Williams, L. B. Kaban, Condylectomy and costochondral graft reconstruction for treatment of active idiopathic condylar resorption. *J. Oral Maxillofac. Surg.* **66**, 65–72 (2008).
3. P. Stoustrup, K. D. Kristensen, A. Küseler, T. K. Pedersen, T. Herlin, Temporomandibular joint steroid injections in patients with juvenile idiopathic arthritis: An observational pilot study on the long-term effect on signs and symptoms. *Pediatr. Rheumatol. Online J.* **13**, 62 (2015).
4. C. Di Blasio, A. Di Blasio, G. Pedrazzi, M. Anghinoni, E. Sesenna, How does the mandible grow after early high condylectomy? *J. Craniofac. Surg.* **26**, 764–771 (2015).
5. R. Fariña, S. Olate, A. Raposo, I. Araya, J. P. Alister, F. Uribe, High condylectomy versus proportional condylectomy: Is secondary orthognathic surgery necessary? *Int. J. Oral Maxillofac. Surg.* **45**, 72–77 (2016).
6. S. Ghawsi, E. Aagaard, T. H. Thygesen, High condylectomy for the treatment of mandibular condylar hyperplasia: A systematic review of the literature. *Int. J. Oral Maxillofac. Surg.* **45**, 60–71 (2016).
7. C. P. Saridin, M. Gilijamse, D. J. Kuik, E. C. te Veldhuis, D. B. Tuinzing, F. Lobbezoo, A. G. Becking, Evaluation of temporomandibular function after high partial condylectomy because of unilateral condylar hyperactivity. *J. Oral Maxillofac. Surg.* **68**, 1094–1099 (2010).
8. M. Bak, A. S. Jacobson, D. Buchbinder, M. L. Urken, Contemporary reconstruction of the mandible. *Oral Oncol.* **46**, 71–76 (2010).
9. C. Schrag, Y.-M. Chang, C.-Y. Tsai, F.-C. Wei, Complete rehabilitation of the mandible following segmental resection. *J. Surg. Oncol.* **94**, 538–545 (2006).
10. R. M. Smith, M. S. Goldwasser, S. R. Sabol, Erosion of a Teflon-Proplast implant into the middle cranial fossa. *J. Oral Maxillofac. Surg.* **51**, 1268–1271 (1993).
11. S. Abramowicz, M. F. Dolwick, S. B. Lewis, C. Dolce, Temporomandibular joint reconstruction after failed Teflon-Proplast implant: Case report and literature review. *Int. J. Oral Maxillofac. Surg.* **37**, 763–767 (2008).
12. A. Boyo, J. McKay, G. Lebovic, D. J. Psutka, Temporomandibular joint total replacement using the Zimmer Biomet Microfixation patient-matched prosthesis results in reduced pain and improved function. *Oral Surg. Oral Med. Oral Pathol. Oral Radiol.* **128**, 572–580 (2019).
13. L. Zou, L. Zhang, D. He, C. Yang, J. Zhao, E. Ellis III, Clinical and radiologic follow-up of Zimmer Biomet stock total temporomandibular joint replacement after surgical modifications. *J. Oral Maxillofac. Surg.* **76**, 2518–2524 (2018).
14. J. Thyssen, T. Menné, Metal allergy—A review on exposures, penetration, genetics, prevalence, and clinical implications. *Chem. Res. Toxicol.* **23**, 309–318 (2009).
15. S. Hassan, L. G. Mercuri, M. Miloro, Does metal hypersensitivity have relevance in patients undergoing TMJ prosthetic replacement? *J. Oral Maxillofac. Surg.* **78**, 908–915 (2020).
16. J. R. Salash, R. H. Hossameldin, A. J. Almarza, J. C. Chou, J. P. McCain, L. G. Mercuri, L. M. Wolford, M. S. Detamore, Potential indications for tissue engineering in temporomandibular joint surgery. *J. Oral Maxillofac. Surg.* **74**, 705–711 (2016).
17. A. M. Tatara, G. L. Koons, E. Watson, T. C. Piepergerdes, S. R. Shah, B. T. Smith, J. Shum, J. C. Melville, I. A. Hanna, N. Demian, T. Ho, A. Ratcliffe, J. J. J. P. van den Beucken, J. A. Jansen, M. E. Wong, A. G. Mikos, Biomaterials-aided mandibular reconstruction using in vivo bioreactors. *Proc. Natl. Acad. Sci. U.S.A.*. **116**, 6954–6963 (2019).
18. O. Guillaume, M. A. Geven, V. Varjas, P. Varga, D. Gehweiler, V. A. Stadelmann, T. Smidt, S. Zeiter, C. Sprecher, R. R. M. Bos, D. W. Grijpma, M. Alini, H. Yuan, G. R. Richards, T. Tang, L. Qin, L. Yuxiao, P. Jiang, D. Eglin, Orbital floor repair using patient specific osteoinductive implant made by stereolithography. *Biomaterials* **233**, 119721 (2020).
19. S. Bhumiratana, J. C. Bernhard, D. M. Alfi, K. Yeager, R. E. Eton, J. Bova, F. Shah, J. M. Gimble, M. J. Lopez, S. B. Eisig, G. Vunjak-Novakovic, Tissue-engineered autologous grafts for facial bone reconstruction. *Sci. Transl. Med.* **8**, 343ra83 (2016).
20. M. E. Elsalanty, D. G. Genecov, Bone grafts in craniofacial surgery. *Craniomaxillofac. Trauma Reconstr.* **2**, 125–134 (2009).
21. S. Bhumiratana, R. E. Eton, S. R. Oungoulian, L. Q. Wan, G. A. Ateshian, G. Vunjak-Novakovic, Large, stratified, and mechanically functional human cartilage grown in vitro by mesenchymal condensation. *Proc. Natl. Acad. Sci. U.S.A.*. **111**, 6940–6945 (2014).
22. S. Bhumiratana, G. Vunjak-Novakovic, Engineering physiologically stiff and stratified human cartilage by fusing condensed mesenchymal stem cells. *Methods* **84**, 109–114 (2015).
23. X. Nie, Y. J. Chuah, W. Zhu, P. He, Y. Peck, D.-A. Wang, Decellularized tissue engineered hyaline cartilage graft for articular cartilage repair. *Biomaterials* **235**, 119821 (2020).
24. M. J. Troulis, J. Glowacki, D. H. Perrott, L. B. Kaban, Effects of latency and rate on bone formation in a porcine mandibular distraction model. *J. Oral Maxillofac. Surg.* **58**, 507–513 (2000).
25. H. Abukawa, H. Terai, D. Hannouche, J. P. Vacanti, L. B. Kaban, M. J. Troulis, Formation of a mandibular condyle in vitro by tissue engineering. *J. Oral Maxillofac. Surg.* **61**, 94–100 (2003).
26. A. J. Almarza, B. N. Brown, B. Arzi, D. F. Ângelo, W. Chung, S. F. Badylak, M. Detamore, Preclinical animal models for temporomandibular joint tissue engineering. *Tissue Eng. Part B Rev.* **24**, 171–178 (2017).
27. W. L. Grayson, D. Marolt, S. Bhumiratana, M. Fröhlich, E. Guo, G. Vunjak-Novakovic, Optimizing the medium perfusion rate in bone tissue engineering bioreactors. *Biotechnol. Bioeng.* **108**, 1159–1170 (2011).
28. M. K. Murphy, D. J. Huey, J. C. Hu, K. A. Athanasiou, TGF-β1, GDF-5, and BMP-2 stimulation induces chondrogenesis in expanded human articular chondrocytes and marrow-derived stromal cells. *Stem Cells* **33**, 762–773 (2015).
29. L. Ruggiero, B. K. Zimmerman, M. Park, L. Han, L. Wang, D. L. Burris, X. L. Lu, Roles of the fibrous superficial zone in the mechanical behavior of TMJ condylar cartilage. *Ann. Biomed. Eng.* **43**, 2652–2662 (2015).
30. J. Lowe, R. Bansal, S. F. Badylak, B. N. Brown, W. L. Chung, A. J. Almarza, Properties of the temporomandibular joint in growing pigs. *J. Biomech. Eng.* **140**, 0710021–0710026 (2018).
31. D. Eyre, Articular cartilage and changes in arthritis: Collagen of articular cartilage. *Arthritis Res.* **4**, 30–35 (2002).
32. L. Wang, M. Lazebnik, M. S. Detamore, Hyaline cartilage cells outperform mandibular condylar cartilage cells in a TMJ fibrocartilage tissue engineering application. *Osteoarthr. Cartil.* **17**, 346–353 (2009).
33. S. Wadhwa, S. Kapila, TMJ disorders: Future innovations in diagnostics and therapeutics. *J. Dent. Educ.* **72**, 930–947 (2008).
34. B. Jones, C. T. Hung, G. A. Ateshian, Biphasic analysis of cartilage stresses in the patellofemoral joint. *J. Knee Surg.* **29**, 92–98 (2016).
35. G. A. Ateshian, V. Rajan, N. O. Chahine, C. E. Canal, C. T. Hung, Modeling the matrix of articular cartilage using a continuous fiber angular distribution predicts many observed phenomena. *J. Biomech. Eng.* **131**, 061003 (2009).
36. FEBio User Manual Version 2.9 (2019); https://help.febio.org/FEBio/FEBio_um_2_9/index.html.
37. E. Tanaka, D. A. Dalla-Bona, T. Iwabe, N. Kawai, E. Yamano, T. van Eijden, M. Tanaka, M. Miyauchi, T. Takata, K. Tanne, The effect of removal of the disc on the friction in the temporomandibular joint. *J. Oral Maxillofac. Surg.* **64**, 1221–1224 (2006).
38. E. Tanaka, N. Kawai, M. Tanaka, M. Todoh, T. van Eijden, K. Hanaoka, D. A. Dalla-Bona, T. Takata, K. Tanne, The frictional coefficient of the temporomandibular joint and its dependency on the magnitude and duration of joint loading. *J. Dent. Res.* **83**, 404–407 (2004).
39. G. Li, J. Yin, J. Gao, T. S. Cheng, N. J. Pavlos, C. Zhang, M. H. Zheng, Subchondral bone in osteoarthritis: Insight into risk factors and microstructural changes. *Arthritis Res. Ther.* **15**, 223 (2013).
40. D. Chen, J. Shen, W. Zhao, T. Wang, L. Han, J. L. Hamilton, H.-J. Im, Osteoarthritis: Toward a comprehensive understanding of pathological mechanism. *Bone Res.* **5**, 16044 (2017).
41. M. M. Stevens, R. P. Marini, D. Schaefer, J. Aronson, R. Langer, V. P. Shastri, In vivo engineering of organs: The bone bioreactor. *Proc. Natl. Acad. Sci. U.S.A.* **102**, 11450–11455 (2005).
42. G. Vunjak-Novakovic, I. Martin, B. Obradovic, S. Treppo, A. J. Grodzinsky, R. Langer, L. E. Freed, Bioreactor cultivation conditions modulate the composition and mechanical properties of tissue-engineered cartilage. *J. Orthop. Res.* **17**, 130–138 (1999).
43. M. Fröhlich, W. L. Grayson, D. Marolt, J. M. Gimble, N. Kregar-Velikonja, G. Vunjak-Novakovic, Bone grafts engineered from human adipose-derived stem cells in perfusion bioreactor culture. *Tissue Eng. Part A* **16**, 179–189 (2010).
44. S. J. Hollister, C. Y. Lin, E. Saito, C. Y. Lin, R. D. Schek, J. M. Taboas, J. M. Williams, B. Partee, C. L. Flanagan, A. Diggs, E. N. Wilke, G. V. Lenthe, R. Müller, T. Wirtz, S. Das, S. E. Feinberg, P. H. Krebsbach, Engineering craniofacial scaffolds. *Orthod. Craniofac. Res.* **8**, 162–173 (2005).
45. N. S. Karp, J. G. McCarthy, J. S. Schreiber, H. A. Sissons, C. H. Thorne, Membranous bone lengthening: A serial histological study. *Ann. Plast. Surg.* **29**, 2–7 (1992).
46. L. Meinel, R. Fajardo, S. Hofmann, R. Langer, J. Chen, B. Snyder, G. Vunjak-Novakovic, D. Kaplan, Silk implants for the healing of critical size bone defects. *Bone* **37**, 688–698 (2005).
47. J. C. Reichert, A. Cipitria, D. R. Epari, S. Saifzadeh, P. Krishnakanth, A. Berner, M. A. Woodruff, H. Schell, M. Mehta, M. A. Schuetz, G. N. Duda, D. W. Hutmacher, A tissue engineering solution for segmental defect regeneration in load-bearing long bones. *Sci. Transl. Med.* **4**, 141ra93 (2012).
48. R. El, R. Rm, Role of subchondral bone in the initiation and progression of cartilage damage. *Clin. Orthop. Relat. Res.* **1986**, 34–40 (1986).
49. N. Shayesteh Moghaddam, A. Jahadakbar, A. Amerinatanzi, M. Elahinia, M. Miller, D. Dean, Metallic fixation of mandibular segmental defects: Graft immobilization and orofacial functional maintenance. *Plast. Reconstr. Surg. Glob. Open* **4**, e858 (2016).

50. C. Loebel, R. L. Mauck, J. A. Burdick, Local nascent protein deposition and remodelling guide mesenchymal stromal cell mechanosensing and fate in three-dimensional hydrogels. *Nat. Mater.* **18**, 883–891 (2019).
51. J. Garvin, J. Qi, M. Maloney, A. J. Banes, Novel system for engineering bioartificial tendons and application of mechanical load. *Tissue Eng.* **9**, 967–979 (2003).
52. K. Ronaldson-Bouchard, S. P. Ma, K. Yeager, T. Chen, L. Song, D. Sirabella, K. Morikawa, D. Teles, M. Yazawa, G. Vunjak-Novakovic, Advanced maturation of human cardiac tissue grown from pluripotent stem cells. *Nature* **556**, 239–243 (2018).
53. D. Seliktar, R. A. Black, R. P. Vito, R. M. Nerem, Dynamic mechanical conditioning of collagen-gel blood vessel constructs induces remodeling in vitro. *Ann. Biomed. Eng.* **28**, 351–362 (2000).
54. D. R. Carter, Mechanical loading histories and cortical bone remodeling. *Calcif. Tissue Int.* **36**, S19–S24 (1984).
55. A. Ruscitto, M. M. Morel, C. J. Shawber, G. Reeve, M. K. Lecholop, D. Bonthius, H. Yao, M. C. Embree, Evidence of vasculature and chondrocyte to osteoblast transdifferentiation in craniofacial synovial joints: Implications for osteoarthritis diagnosis and therapy. *FASEB J.* **34**, 4445–4461 (2020).
56. K. Legemate, S. Tarafder, Y. Jun, C. H. Lee, Engineering human TMJ discs with protein-releasing 3D-printed scaffolds. *J. Dent. Res.* **95**, 800–807 (2016).
57. N. Vapniarsky, L. W. Huwe, B. Arzi, M. K. Houghton, M. E. Wong, J. W. Wilson, D. C. Hatcher, J. C. Hu, K. A. Athanasiou, Tissue engineering toward temporomandibular joint disc regeneration. *Sci. Transl. Med.* **10**, eaaq1802 (2018).
58. C. Kermer, F. Ziya-Ghazvini, P. W. Poeschl, C. Klug, Two stage reconstruction with revascularized grafts after resection of retromolar and oropharyngeal carcinoma. *Int. J. Oral Maxillofac. Surg.* **33**, 554–557 (2004).
59. D. Rohner, C. Jaquiéry, C. Kunz, P. Bucher, H. Maas, B. Hammer, Maxillofacial reconstruction with prefabricated osseous free flaps: A 3-year experience with 24 patients. *Plast. Reconstr. Surg.* **112**, 748–757 (2003).
60. K. Le Blanc, C. Tammik, K. Rosendahl, E. Zetterberg, O. Ringdén, HLA expression and immunologic properties of differentiated and undifferentiated mesenchymal stem cells. *Exp. Hematol.* **31**, 890–896 (2003).
61. H. J. Motulsky, R. E. Brown, Detecting outliers when fitting data with nonlinear regression – A new method based on robust nonlinear regression and the false discovery rate. *BMC Bioinformatics* **7**, 123 (2006).
62. K. J. Williams, A. A. Picou, S. L. Kish, A. M. Giraldo, R. A. Godke, K. R. Bondioli, Isolation and characterization of porcine adipose tissue-derived adult stem cells. *Cells Tissues Organs* **188**, 251–258 (2008).
63. W. L. Grayson, S. Bhumiratana, C. Cannizzaro, P.-H. G. Chao, D. P. Lennon, A. I. Caplan, G. Vunjak-Novakovic, Effects of initial seeding density and fluid perfusion rate on formation of tissue-engineered bone. *Tissue Eng. Part A* **14**, 1809–1820 (2008).
64. W. L. Grayson, M. Fröhlich, K. Yeager, S. Bhumiratana, M. E. Chan, C. Cannizzaro, L. Q. Wan, X. S. Liu, X. E. Guo, G. Vunjak-Novakovic, Engineering anatomically shaped human bone grafts. *Proc. Natl. Acad. Sci. U.S.A.* **107**, 3299–3304 (2010).
65. Hematologic reference ranges - Special subjects, in *Merck Veterinary Manual* (1955); www.merckvetmanual.com/special-subjects/reference-guides/hematologic-reference-ranges.
66. Serum biochemical reference ranges - Special subjects, in *Merck Veterinary Manual* (1955); www.merckvetmanual.com/special-subjects/reference-guides/serum-biochemical-reference-ranges.
67. S. R. Oungoulian, K. M. Durney, B. K. Jones, C. S. Ahmad, C. T. Hung, G. A. Ateshian, Wear and damage of articular cartilage with friction against orthopedic implant materials. *J. Biomech.* **48**, 1957–1964 (2015).
68. R. L. Mauck, M. A. Soltz, C. C. B. Wang, D. D. Wong, P.-H. G. Chao, W. B. Valhmu, C. T. Hung, G. A. Ateshian, Functional tissue engineering of articular cartilage through dynamic loading of chondrocyte-seeded agarose gels. *J. Biomech. Eng.* **122**, 252–260 (2000).
69. X. Chen, B. K. Zimmerman, X. L. Lu, Determine the equilibrium mechanical properties of articular cartilage from the short-term indentation response. *J. Biomech.* **48**, 176–180 (2015).
70. B. K. Zimmerman, E. D. Bonnevie, M. Park, Y. Zhou, L. Wang, D. L. Burris, X. L. Lu, Role of interstitial fluid pressurization in TMJ lubrication. *J. Dent. Res.* **94**, 85–92 (2015).
71. S. A. Maas, B. J. Ellis, G. A. Ateshian, J. A. Weiss, FEBio: Finite elements for biomechanics. *J. Biomech. Eng.* **134**, 011005 (2012).
72. G. A. Ateshian, S. Maas, J. A. Weiss, Finite element algorithm for frictionless contact of porous permeable media under finite deformation and sliding. *J. Biomech. Eng.* **132**, 061006 (2010).
73. J. Katta, Z. Jin, E. Ingham, J. Fisher, Biotribology of articular cartilage—A review of the recent advances. *Med. Eng. Phys.* **30**, 1349–1363 (2008).
74. E. Tanaka, F. Pelayo, N. Kim, M. J. Lamela, N. Kawai, A. Fernández-Canteli, Stress relaxation behaviors of articular cartilages in porcine temporomandibular joint. *J. Biomech.* **47**, 1582–1587 (2014).
75. X. L. Lu, V. C. Mow, X. E. Guo, Proteoglycans and mechanical behavior of condylar cartilage. *J. Dent. Res.* **88**, 244–248 (2009).
76. K.-W. Kim, M. E. Wong, J. F. Helfrick, J. B. Thomas, K. A. Athanasiou, Biomechanical tissue characterization of the superior joint space of the porcine temporomandibular joint. *Ann. Biomed. Eng.* **31**, 924–930 (2003).

Acknowledgments: We thank the staff at LaCell LLC (A. Alarcon Uquillas, X. Wu, and T. Frazier) for assistance in preparing the porcine ASCs, the residents at the Columbia University College of Dental Medicine (M. Perrino, T. Kunkle, M. Forman, and T. Zenga) for assistance in animal surgeries, and the staff at the Louisiana State University School of Veterinary Study for veterinary assistance. We thank S. Stylianos and M. Summers for assistance in conducting flow analyses and fabricating the bioreactors and scaffolds. We thank J. Zhou for assistance with preparing and culturing the grafts and with analyses. **Funding:** We acknowledge the funding support of this work by the NIH (grants EB027062 and DE016525 to G.V.-N. and GM083925 to G.A.A.), the National Science Foundation Graduate Research Fellowship (grant no. 1644869 to J.Y.W.), and the Department of Defense (grant W81XWH-19-PRMRP-IIRA to G.A.A.). **Author contributions:** D.C., K.M.K., J.Y.W., J.C.B., J.J.N., and G.V.-N. designed experiments and developed the animal model. D.C., J.Y.W., K.M.K., and G.V.-N. wrote the paper. D.C., K.M.K., J.Y.W., J.C.B., J.J.N., and K.Y. conducted flow analyses, bioreactor design and fabrication, and bone scaffold manufacturing. J.M.G. isolated and characterized ASCs. O.F.V. tagged cells for fluorescence. D.C., K.M.K., J.Y.W., J.C.B., and J.J.N. were responsible for cell preparation and bioreactor culture. D.C., K.M.K., and J.Y.W. were responsible for histology, immunohistochemistry, and oxytetracycline imaging. D.C., K.M.D., B.K.Z., C.S., K.M.K., and G.A.A. performed friction and compression testing and analysis. D.C., K.Y., S.R., and X.E.G. performed CT and μCT reconstruction and analysis. M.J.L. and S.B.E. performed animal surgery. M.J.L. and C.T. harvested adipose tissue, performed oxytetracycline injections, and oversaw animal care. **Competing interests:** J.M.G. is inventor on a patent application (US20140017783, 2014) related to isolation of adipose stem cells using nonenzymatic methods, which was not used in the study. G.V.N. is inventor on a provisional patent application (US 14/782,630, 2015) related to the bone tissue engineering. The technology described in this paper is now being commercialized through a Columbia University spinout, EpiBone, where G.V.-N. is a cofounder and Board member and S.B.E. has an advisory role. J.M.G. is a co-owner, cofounder, and chief scientific officer of LaCell LLC, a company focusing on stem cell technology and clinical translation. The authors confirm that none of the affiliations listed directly benefits from this research. **Data and materials availability:** All data are included in the paper and the Supplementary Materials.

Submitted 14 April 2020
Accepted 16 September 2020
Published 14 October 2020
10.1126/scitranslmed.abb6683

Citation: D. Chen, J. Y. Wu, K. M. Kennedy, K. Yeager, J. C. Bernhard, J. J. Ng, B. K. Zimmerman, S. Robinson, K. M. Durney, C. Shaeffer, O. F. Vila, C. Takawira, J. M. Gimble, X. E. Guo, G. A. Ateshian, M. J. Lopez, S. B. Eisig, G. Vunjak-Novakovic, Tissue engineered autologous cartilage-bone grafts for temporomandibular joint regeneration. *Sci. Transl. Med.* **12**, eabb6683 (2020).

Science Translational Medicine

Tissue engineered autologous cartilage-bone grafts for temporomandibular joint regeneration

David Chen, Josephine Y. Wu, Kelsey M. Kennedy, Keith Yeager, Jonathan C. Bernhard, Johnathan J. Ng, Brandon K. Zimmerman, Samuel Robinson, Krista M. Durney, Courtney Shaeffer, Olaia F. Vila, Catherine Takawira, Jeffrey M. Gimble, X. Edward Guo, Gerard A. Ateshian, Mandi J. Lopez, Sidney B. Eisig and Gordana Vunjak-Novakovic

Sci Transl Med **12**, eabb6683.
DOI: 10.1126/scitranslmed.abb6683

Tempering troublesome joints

Temporomandibular joint (TMJ) dysfunction is a common affliction of the jaw that can cause painful interference with chewing or movement, sometimes requiring surgical intervention. Chen *et al.* sought to reconstruct the cartilage and bone components of the ramus-condyle unit of the TMJ. Using bioreactor culture of autologous cells, they showed that engineered complex tissue grafts repaired TMJ defects in minipigs over 6 months. Results demonstrate the importance of regeneration of the cartilage layer overlying the bone of the constructs for recapitulation of native-like tissue morphology and biochemical composition, as well as long-term function.

Science Translational Medicine (ISSN 1946-6242) is published by the American Association for the Advancement of Science, 1200 New York Avenue NW, Washington, DC 20005. The title *Science Translational Medicine* is a registered trademark of AAAS.